LAWRENCE
LIVERMORE
NATIONAL
LABORATORY

LLNL-TR-460956

Application of Ensemble Sensitivity Analysis to Observation Targeting for Short-term Wind Speed Forecasting in the Tehachapi Region Winter Season

J. Zack, E. Natenberg, S. Young, G. Van Knowe, K. Waight, J. Manobainco, C. Kamath

October 22, 2010

Disclaimer

This work performed under the auspices of the U.S. Department of Energy by Lawrence Livermore National Laboratory under Contract DE-AC52-07NA27344.

Application of Ensemble Sensitivity Analysis to Observation Targeting for Short-term Wind Speed Forecasting in the Tehachapi Region Winter Season

John Zack, Eddie Natenberg, Steve Young, Glenn Van Knowe,
Ken Waight, John Manobianco
AWS Truepower, LLC

Chandrika Kamath
Lawrence Livermore National Laboratory

20 October 2010

1. Introduction

This study extends the wind power forecast sensitivity work done by Zack et al. (2010a, b) in two prior research efforts. Zack et al. (2010a, b) investigated the relative predictive value and optimal combination of different variables/locations from correlated sensitivity patterns. Their work involved developing the Multiple Observation Optimization Algorithm (MOOA) and applying the algorithm to the results obtained from the Ensemble Sensitivity Analysis (ESA) method (Ancell and Hakim 2007; Torn and Hakim 2008).

In the previous two studies (Zack et al. 2010a, b), the ESA-MOOA approach was evaluated for the wind plants in the Tehachapi Pass, CA and Mid-Columbia Basin, WA regions for periods during the warm season. Both studies demonstrated that forecast sensitivity was characterized by well-defined, localized patterns for a number of state variables such as the 80-m wind and the 25-m to 1-km temperature difference prior to the forecast time. The forecasted sensitivities were consistent with the basic physical processes responsible for wind patterns in the respective regions.

In the current project, the ESA-MOOA approach is applied to the cold season (1 January to 18 February 2010) for the wind plants located in the Tehachapi Pass as shown in Figure 1.

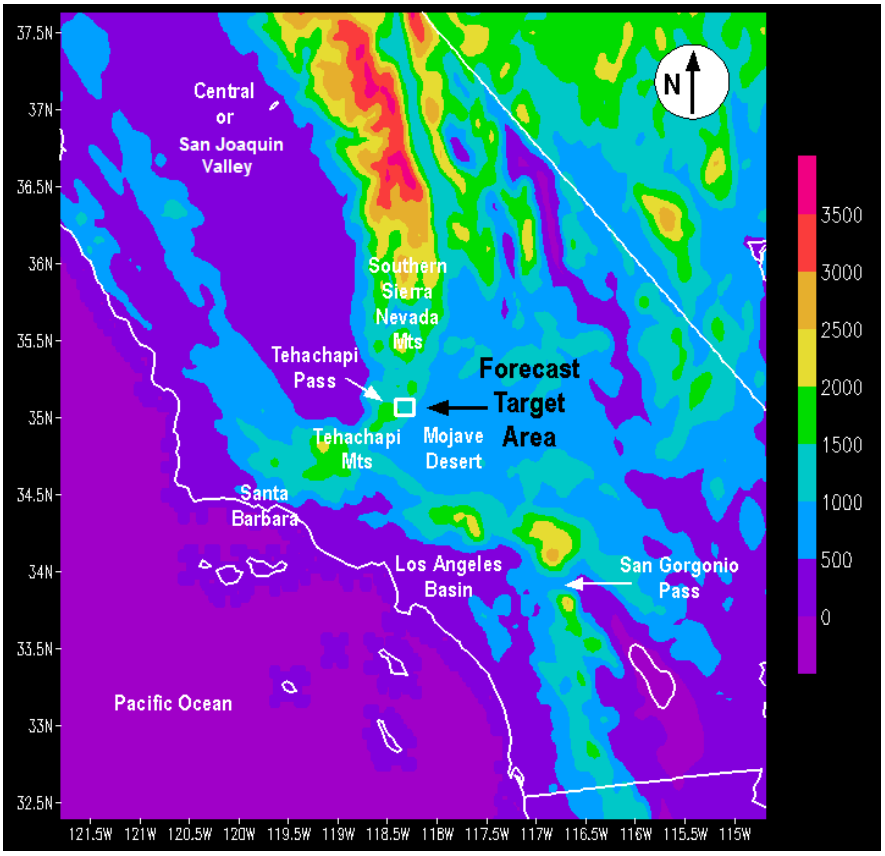

Figure 1. *The geographical area covered by the model grid domain used in the Tehachapi Pass ensemble sensitivity experiments. The color shading depicts the terrain elevation (m) on the scale of the model grid. The white box denotes the forecast target area.*

The objectives for this study were to identify measurement locations and variables that have the greatest positive impact on the accuracy of wind forecasts in the 0- to 6-hour look-ahead periods for the Tehachapi Pass wind generation area during the cold season and to establish a higher level of confidence in the ESA-MOOA for mesoscale applications.

The report is organized as follows. Section 2 provides an overview of the methodology, Section 3 highlights ensemble factors that impacted the results, Section 4 presents single-variable results, Section 5 covers multiple variable results, and Section 6 concludes with a summary and discussion of future work.

2. Methods

The following subsections provide a brief overview of the methods used in this study. Zack et al. (2010a, b) describes the methodology in more detail.

2.1 Description of ESA and EnKF

ESA and the ensemble Kalman filter (EnKF) are the key methods used to evaluate sensitivity in this study. The ESA approach uses data generated by a set (ensemble) of perturbed numerical weather prediction (NWP) simulations for a sample time period to diagnose the sensitivity of a specified forecast variable (metric) for a target location to initial condition (IC) state variable(s) at other locations and prior times. The ensemble of NWP simulations is produced by starting with a single initial state at the beginning of the analysis period and introducing statistical perturbations into the initial and lateral boundary conditions. For subsequent simulations, the initial state is a combination of the predicted and observed state. This process generates a set of simulations that differ from each other due to the perturbations. The number of simulations must be large enough to produce a statistically significant sample for the sensitivity calculations. Past studies have used 48 or more ensemble members for large-scale ESA applications (Torn and Hakim 2008).

The evaluation of simulation "spread" or differences between individual members of the ensemble was accomplished using EnKF (Houtekamer and Mitchell 1998; Evensen 2007). The EnKF attempts to balance the predicted and observed state of the atmosphere by estimating the likelihood of each state at any given time over the entire set of simulations in the ensemble. The EnKF assumes that model errors follow a normal (Gaussian) distribution in order to determine the most probable state of the atmosphere.

The error was assessed using the time-dependent spread and deviations obtained from the ensemble state with that of the observed state. Ensemble members are allowed to integrate forward in time while the filter monitors the spread in the ensemble. The EnKF assesses predictabilities (likelihood of occurrence) of the variable of interest for the target area by monitoring the change in the spread of the NWP ensemble.

2.2 Model Configuration

The NWP simulations were generated on a three-dimensional matrix of 200 x 200 x 39 points with 4-km spacing centered over southern California. This grid is identical to the one used for the summer Tehachapi Pass simulations (Zack et al. 2010a). The vertical grid spacing increases

with height so that there is higher resolution near the surface of the earth. Appendix B includes a table that lists the vertical levels.

The simulations were produced using version 2.2 of the Weather Research and Forecast (WRF) atmospheric model (Skamarock et al. 2005). Observational data were assimilated every 6 hours using an EnKF data assimilation procedure within the Data Assimilation Research Testbed (DART) software (Anderson 2001; Anderson et al. 2009). Data from the Rapid Update Cycle (RUC) model were used for initial and lateral boundary conditions. A total of 48 ensemble members were used in the analysis. Appendix A contains additional details of the (1) WRF model configuration, (2) EnKF data assimilation system, and (3) data types assimilated.

The simulations extended from 0000 UTC 1 January to 0300 UTC 18 February 2010. This period fell near the end of a weak to moderate El Niño phase of the El Niño-Southern Oscillation (ENSO). Studies have demonstrated that there is a connection to the frequency and strength of the large scale low pressure systems that impact the Tehachapi Pass region in the winter and the phase of ENSO (Monteverdi and Null 1998). Thus the phase of ENSO would seem to be a relevant factor in the climatological sensitivity relationship between the IC variables to the variability of wind speed at the target location. To answer this question, experiments would need to be performed for winters in different phases of ENSO.

The first two days were designated as a "spin-up" period and the data were not used in the sensitivity calculations. Therefore, the analysis period covered 46 days from 3 January to 18 February 2010. The simulation period consisted of 6-hour simulations with data assimilation at the beginning of each period. A 6-hour cycle between data assimilation was chosen to allow the model enough time to adjust to the ingested observational data.

The sensitivities were calculated for two separate time periods from 0 to 3 hours and from 3 to 6 hours. The 3-hour sensitivities were computed because this is the look-ahead period of greatest interest to the grid operators. The 3- to 6-hour sensitivities were also computed for each forecast in order to provide additional independent time periods to evaluate. The 1-hour sensitivities were computed from the initial time to hour 1 and from hour 3 to hour 4 of each simulation.

2.3 Description of IC Variables

The forecast metric (F) was defined as the average 80-m wind speed above ground level (AGL) over the target area shown in Figure 1. The sensitivity calculation is not restricted to the same variable used to define the forecast metric. Sensitivity values were calculated and evaluated for the thirteen IC state variables listed in Table 1.

The IC variables can be grouped into three categories: (1) Single level sensitivities, which include wind speed at various levels and 2-m temperature, (2) vertical wind shear, and (3) vertical temperature gradient. The wind shear and temperature gradients were computed for various layers from near the surface to a level of 2-km AGL.

2.4 Description of Statistical Quantities Used to Evaluate Sensitivity

Three statistical quantities are used to qualify and quantify the relationship between the evaluation IC variables and correlation of those variables to the 80-m wind (metric variable) at the target location: (1) sensitivity, (2) frequency of significant sensitivity, and (3) coefficient of

determination (R^2). These statistical quantities and methods of calculation are described fully in Zack et al. (2010a, b).

The sensitivity relationship is expressed as:

$$\frac{\partial F}{\partial s} = \frac{\mathrm{cov}(F,s)}{\mathrm{var}(s)} \tag{1}$$

where $\partial F/\partial s$ is defined as the sensitivity of a target forecast metric variable (F) to selected IC state variables (s) from prior simulated times at all points in the model domain. The covariance (cov) and variance (var) are computed over all ensemble members (Ancell and Hakim 2007). The sensitivity can be thought of as the slope of a linear relationship between the IC variable and the forecasted variable. A higher absolute sensitivity value means that a given change in the IC variable will lead to a larger change in the variable being forecasted.

The average was constructed for all dates and times in the analysis period to obtain information about which areas have the highest average sensitivity over all cases. In addition, the average was computed for periods with the largest ensemble variance in the forecast metric. This approach yields information about the locations and variables that have the most sensitivity for those types of events. Details of how the computations were made for the ensembles with the largest variance are presented in Section 2.6.

Table 1. Thirteen IC state variables used in the evaluation of sensitivity.

Wind Speed Related
80-m AGL wind speed
250-m AGL wind speed
1.5-km above mean sea level (AMSL) wind speed
3-km AMSL wind speed
Wind Shear Related
10-m to 80-m AGL wind shear
80-m to 500-m AGL wind shear
500-m to 1-km AGL wind shear
Temperature Related
2-m AGL temperature
2-m to 80-m AGL temperature difference
80-m to 1-km AGL temperature difference
80-m to 500-m AGL temperature difference
500-m to 1-km AGL temperature difference
1-km to 2-km AGL temperature difference

2.5 Location and Variable Combinations

The forecast sensitivity dataset can be used to select a combination of locations and variables that will provide the most improvement for the prediction of the forecast metric over the desired look-ahead period. Typically, the direct use of the most sensitive points would not likely yield an optimal solution because the IC variables, in general, have a significant degree of correlation. Even though a number of variables may exhibit a high degree of sensitivity, much of the "predictive" information in each variable is highly correlated with the information in other variables. Therefore, many of the highly sensitive variables/locations essentially provide redundant information about the variability of the forecast metric for a given look-ahead period.

In order to address this issue, the MOOA (Zack et al. 2010a, b) was used to determine the relative predictive value of different combinations of variables/locations. In this procedure, a small set of variables/locations is selected by a separate algorithm and then multiple linear regression is performed on all combinations of variables/locations within that set.

In the Tehachapi Pass warm season study (Zack et al. 2010a), the maximum average sensitivity magnitude was used as the criteria to select locations for the set of variables used in the MOOA. The locations of the maximum average R^2 value were chosen in this study because previous efforts (Zack et al. 2010a, b) suggest that R^2 patterns were a better indicator of which combinations and individual variables/locations have the most value for a given forecast look-ahead period.

In an effort to improve the results from the previous studies (Zack et al. 2010a, b), four instead of three variables are used in the regression calculations for both the 1- and 3-hour look-ahead times. The variables are normalized prior to the regression. The normalization permits the regression coefficients to be used as an indicator of the relative importance of each variable when combined with other variables in the set. The R^2 values of each multiple regression can also be used as an indicator of which combinations and individual variables/locations have the most value for a given forecast look-ahead period.

2.6 High Ensemble Variance Sensitivities

To examine further the impact of ensemble variance on the sensitivity results, a subsample of cases was chosen to assess results for only those cases that had high ensemble variance. Table 2 lists 73 unique 3-hour periods that were chosen from the results (presented in Section 4) to compute 3-hour look-ahead sensitivities for the metric location. These cases included both times of observed and simulated ramps as well as times of little to no wind speed change. The observed ramps were determined by looking at five private meteorological (met) tower data in the Tehachapi pass area. Both observed met tower and simulated ensemble data were used to determine the ramp periods. To be considered part of the high variance dataset ensemble, simulated variance had to be ~1 m/s for 80 meter wind speed at the metric location for more than one assimilation cycle (greater than 6 hours) shown in Figures 3 and 4.

This increased ensemble spread represents a greater amount of uncertainty in the forecasted state within the ensemble. It is thought to produce a more representative assessment of the impact of each initial condition parameter, as shown by better spatial patterns in the sensitivities and higher R^2 values for the single variable regressions. The need for a higher variance dataset is discussed

in Section 3 while the results for the single and multivariate analyses are discussed in Sections 4 and 5, respectively.

Table 2. Summary of the 73 high variance period cases for Tehachapi Pass.

Date	Valid Metric Time (UTC)
1/10/10	00,03,21
1/11/10	00
1/13/10	00,03,12,18
1/14/10	00,03,06,09,12,15
1/18/10	12,
1/19/10	06,09,12,18,21
1/20/10	00,06,09,12,18
1/21/10	06,09,15,18,21
1/22/10	09,12,15,18,21
1/23/10	00,03,06,09,12,15,18,21
1/24/10	00,03,06,09,12
2/5/10	18
2/6/10	00,03,06,09,12,15,18,21
2/7/10	00,03,06,09,12,15,18,21
2/8/10	00,03,06,09
2/9/10	21
2/10/10	00,12,15

3. Ensemble Factors Impacting Results

The was a noted lack of ensemble spread in the Tehachapi winter season low simulations when compared with the Tehachapi and Mid-Columbia warm season experiments (Fig. 2). The question of whether the ensemble spread was representative of the true variability (uncertainty) was addressed by comparing wind speed observations made in the local area with values from the ensemble members. The fact that observations are frequently well outside the range of simulated wind speeds indicates that the ensemble is not capturing the true uncertainty and is generally underdispersive.

The lack of ensemble spread in both the metric variable (80-m wind speed at the target location) and the thirteen IC variables (throughout the grid) was a significant factor that impacted the interpretation of the Tehachapi winter simulation experiments. The following discussion explains how the lack of ensemble spread impacted the results and may have been caused by the perturbation technique.

The winter season low ensemble spread was considerably different from what was observed in the Tehachapi and Mid-Columbia warm season experiments. The results for both warm season sensitivity experiments exhibited significant ensemble spread in the 80-m wind speed on the order of several meters per second in the metric box. The summer season sensitivities showed patterns that were meaningful from a meteorological perspective. These patterns were coherent

and consistent with the existing knowledge of basic physical processes associated with diurnally driven terrain flows that dominate the Tehachapi region in the summer season. Ensemble divergence was greatest in areas of elevated terrain related to terrain forced circulations in the Tehachapi region.

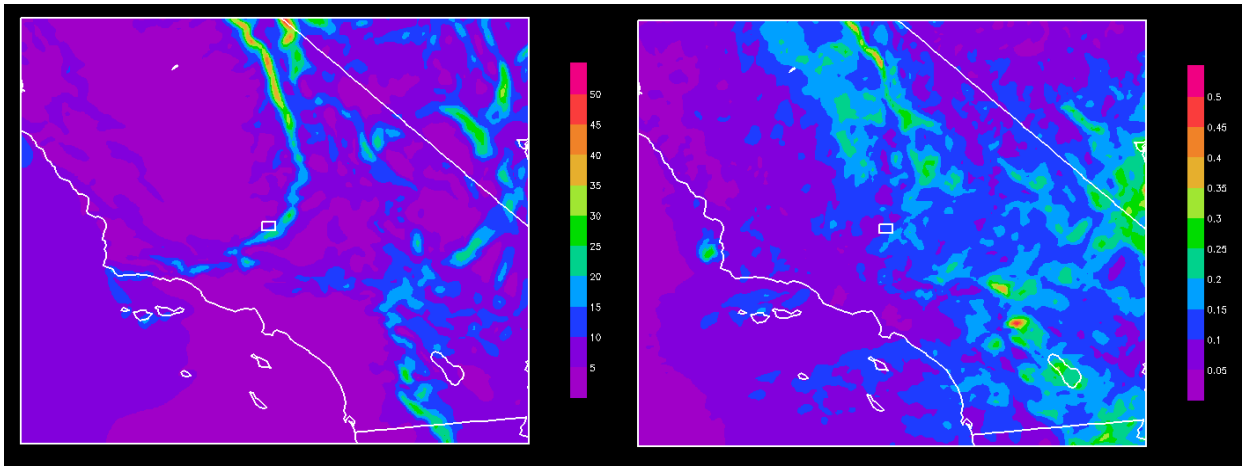

Figure 2. *Comparison of average variance of 80-m wind speed (m^2/s^2) throughout the entire domain for all time periods in 46-day analysis period for Tehachapi Pass for the summer (left) and winter (right). Note that the scale extends from 0 to 50 on the left, and 0 to 0.5 on the right.*

In contrast to the summer results, the interpretation of the Tehachapi winter results was limited by low ensemble spread in the wind speed forecast for the metric location (Fig. 3). The Tehachapi winter average ensemble standard deviation was only 0.12 m/s for the entire 46-day period. With the exception of a few hours around 0000 UTC on January 20, all ensemble members predicted a nearly identical sequence, timing, and to a lesser extent, amplitude of wind ramping events (Fig. 4). This pattern prevailed even when the ensemble had significant errors in predicting ramping events, such as on 19-20 January and 26-29 January (Fig. 4).

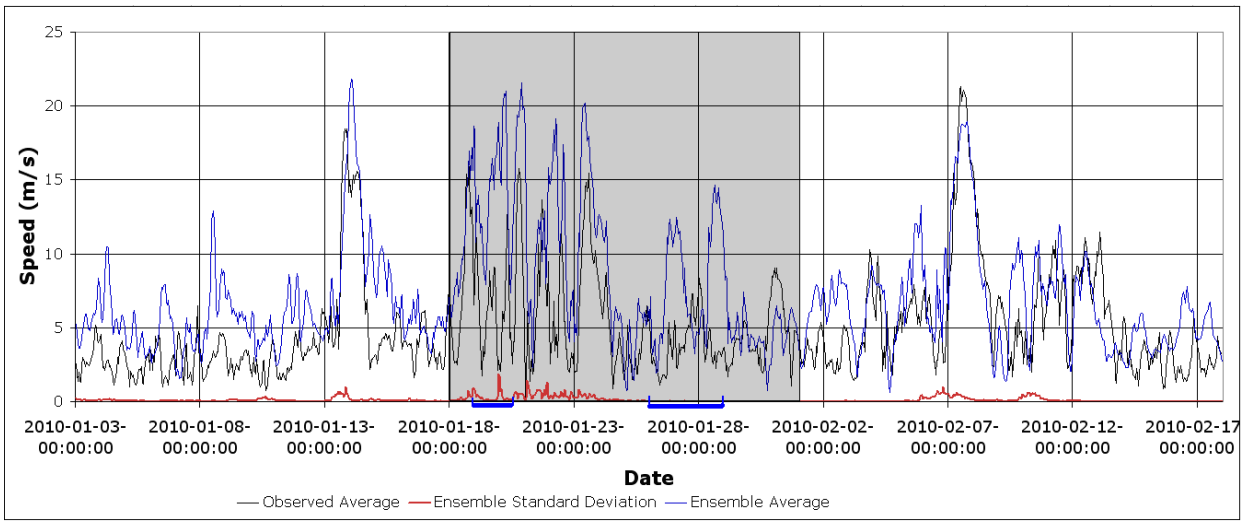

Figure 3. *Ensemble 80-m mean wind speed (blue line), 80-m wind speed standard deviation (red line) and observed 5-tower 30-m mean wind speed (black line) in the Tehachapi pass area for the entire 46-day sample. The gray shading shows the expanded period in Figure 4. The average ensemble standard deviation for the entire period is 0.12 m/s. The periods of 19-20 and 26-29 January referenced in the text are depicted by a thick blue line on the date axis. The period shaded in gray is shown in Figure 4.*

In the Tehachapi Pass winter simulations there was also a noticeable lack of ensemble spread for all thirteen initial condition variables over the majority of times during the 46-day analysis period. Overall, the magnitude of the sensitivities for the full 46-day period was much lower than that for the summer Tehachapi and Mid-Columbia Basin experiments.

As shown in Equation 1, the sensitivity is the slope of the regression that approximates the correlation between the change in the IC state variable and the metric variable. It consists of the ratio of the covariance between the IC state variable and the forecast metric (the numerator) to the variance of the IC state variable (the denominator). Low variance in the IC state variable for the winter case decreases the magnitude of the denominator. As a result of the mathematical relationship between the numerator and denominator, small changes in the covariance between the forecast metric to the initial condition (numerator term) and the variance of the initial condition (denominator term) can lead to large changes in the sensitivity value.

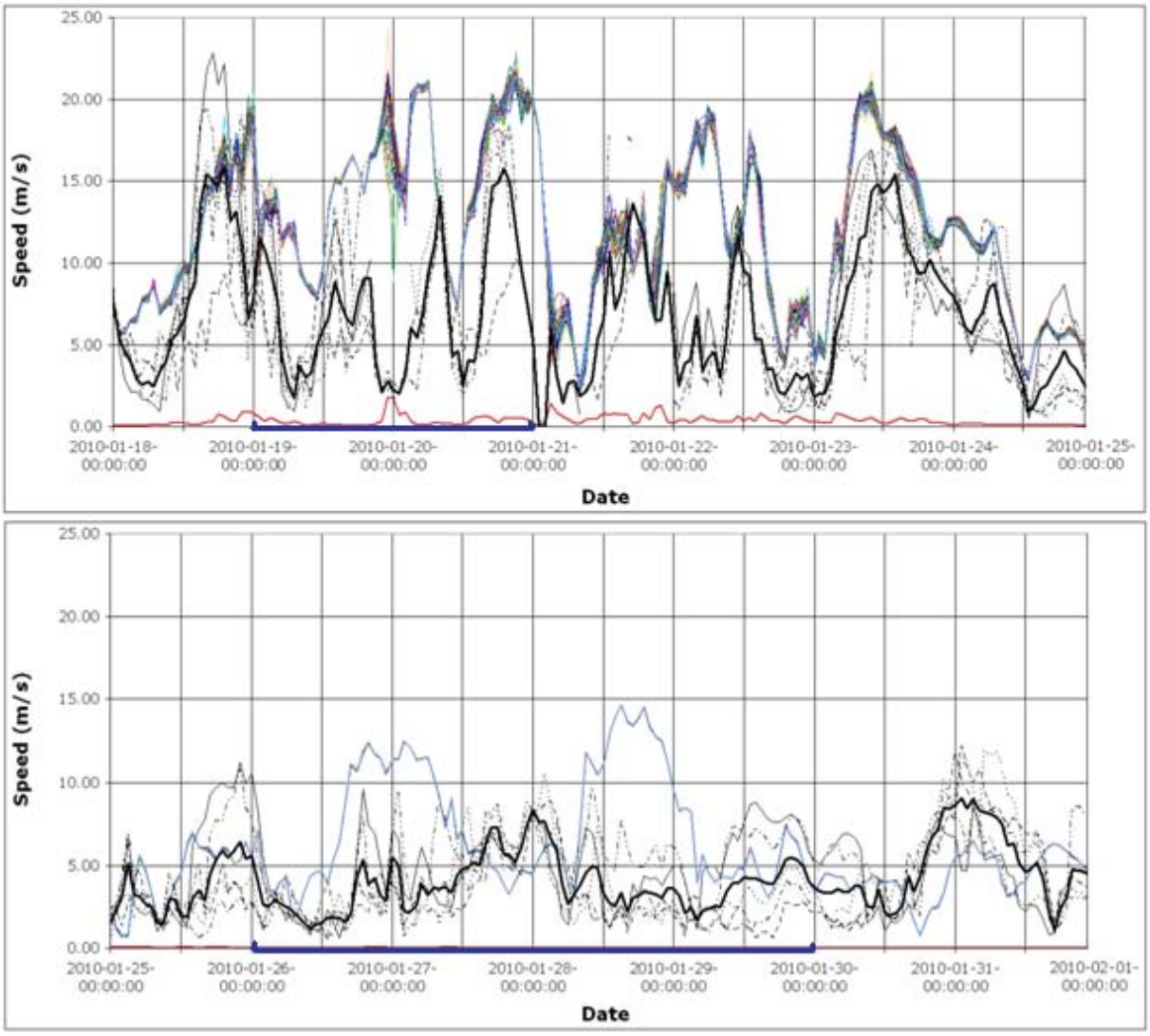

Figure 4. *Observed and ensemble predicted wind speed in the metric box for 18-24 January 2010 (top) and 25-31 January 2010 (bottom) with time in UTC. Ensemble standard deviation appears as a red line at the bottom of each graph. Ensemble members appear as a blue line when the spread is small and a colored band when it is larger. A few individual members diverge from the mean enough to appear individually (gold and green lines) only around 0000 UTC on January 20. Black lines with various dash and dot patterns depict observations at each of the five 30-m towers in the Tehachapi pass area. The thick black line depicts the average observational values of the five towers. The periods of 19-20 and 26-29 January referenced in the text are depicted by a thick blue line on the date axis.*

Both the variance and covariance terms exhibited generally low values. Figure 2 shows that the mean winter variance of the 80-m wind speed IC state variable over the entire domain was approximately two orders of magnitude smaller than the summer variance. The relatively weak signal in the variance of the IC state variable found in this study typically resulted in scattered high and low sensitivity values (Fig. 5). This issue caused noisy spatial sensitivity patterns, low

R^2, and low significant sensitivity frequency (as discussed in Section 4). The uncertainty also makes it more difficult to interpret the results and develop a meaningful meteorological explanation.

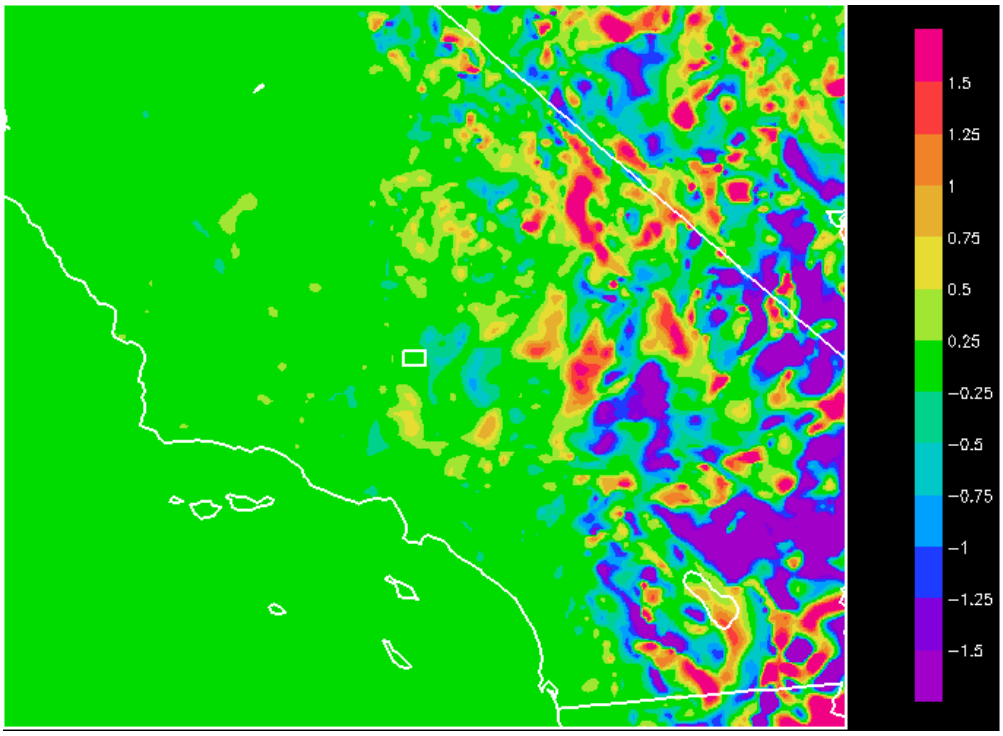

Figure 5. *Sensitivity of average 80-m wind speed in the white box (forecast metric box) at 0300 UTC 3 February to 80-m wind speed three hours earlier.*

The widely varying sensitivities as well as low R^2 and significant sensitivity frequency seemed to be due to the general convergence of the ensemble, which manifested itself as low ensemble spread. The lack of spread may have been at least partly due to the generally weaker surface flow regime that dominated this period. Also, the lack of a diurnally-forced weather regime had a negative impact on resolving higher magnitude sensitivities when computing averages. Assuming the spread accurately represents the uncertainty, the smaller spread among the ensemble members would indicate an increased amount of certainty in the forecasted state for the winter period. Observations then should have little impact on the NWP forecasted state due to ensemble convergence and the general low spread of the metric and initial condition variable state in the winter. However, it is possible that the true uncertainty was larger than the ensemble spread suggested.

Ideally, ensemble spread is proportional to the uncertainty in the model prediction. Spread is maintained by introducing perturbations into the boundary conditions of each member at periodic intervals. In an ideal situation, the perturbations neither amplify in an unstable manner nor rapidly dampen. Amplification can lead to model instability while rapid dampening leads to ensemble convergence and insufficient spread.

The statistics presented in Figures 3 and 4 suggest that perturbations introduced into the

ensemble through the external boundary conditions rapidly dampened as they moved into the interior of the domain, resulting in insufficient ensemble spread. There are many times when the ensemble spread of the forecast metric is very small, implying low uncertainty in the forecast Fig. 3). However, the observations at the metric location are very different from the narrow consensus of ensemble members.

The perturbation techniques used to generate the ensembles were identical for the Tehachapi winter and Mid-Columbia summer experiments (Zack et al. 2010b). On the other hand, the Tehachapi summer ensemble used a smaller horizontal correlation parameter to compute the perturbations (Zack et al. 2010a). However, the Mid-Columbia ensemble was run with an inner nested grid and an outer grid while the Tehachapi ensembles included only a single high-resolution grid. Since the perturbations for the Mid-Columbia ensemble were introduced on the outer grid, they were significantly farther from the area of interest than the perturbations introduced in the Tehachapi winter ensemble. Even with the differences in perturbation and nesting techniques, both the Mid-Columbia and Tehachapi summer ensembles did have sufficient spread and meaningful results.

Based on the above analysis, the results indicate that the growth and decay of perturbations varies primarily because of three factors:

(1) amplitude and spatial extent of the perturbations,
(2) type of weather regime, and
(3) model grid parameters.

Some combination of these factors most likely caused the low ensemble spread in the Tehachapi winter regime. For perturbations to amplify in the ensemble, their spatial size must match modes within the ensemble that are uncertain and the spatial extent of the perturbations must be large enough to induce spread in both the first set of initial conditions and the boundary conditions for every forecast interval. For the Mid-Columbia ensemble (Zack et al. 2010b), the spatial extent of the perturbed boundaries were large enough to cause adequate ensemble divergence, but these settings were likely not adequate to induce enough spread in the non-nested Tehachapi winter runs.

4. Single-Variable Results

This section discusses the spatial variation of sensitivity, R^2, and frequency of significant sensitivity for some of the variables listed in Table 1. Section 5 discusses the use of the MOOA technique to find optimal combinations of variables and locations.

4.1 Winter and Summer Differences

The flow in the Tehachapi Pass for the time period examined was dominated by two sets of large-scale weather patterns. One pattern involved strong synoptic scale low pressure systems moving through the mid California region associated with a strong upper-tropospheric polar jet stream near or over the target region (Figure 6, upper left and right panels). The other pattern occurred when the upper tropospheric jet stream was displaced north of the target area resulting in weak synoptic forcing (Figure 6, lower left and right panels). The mesoscale forcing was very weak during this period. In addition, the land-ocean temperature difference was quite small, so

diurnally-forced sea breeze circulations were relatively weak. This regime was very different from the summer when the synoptic pattern was consistently weak and the diurnally-forced circulations were much stronger.

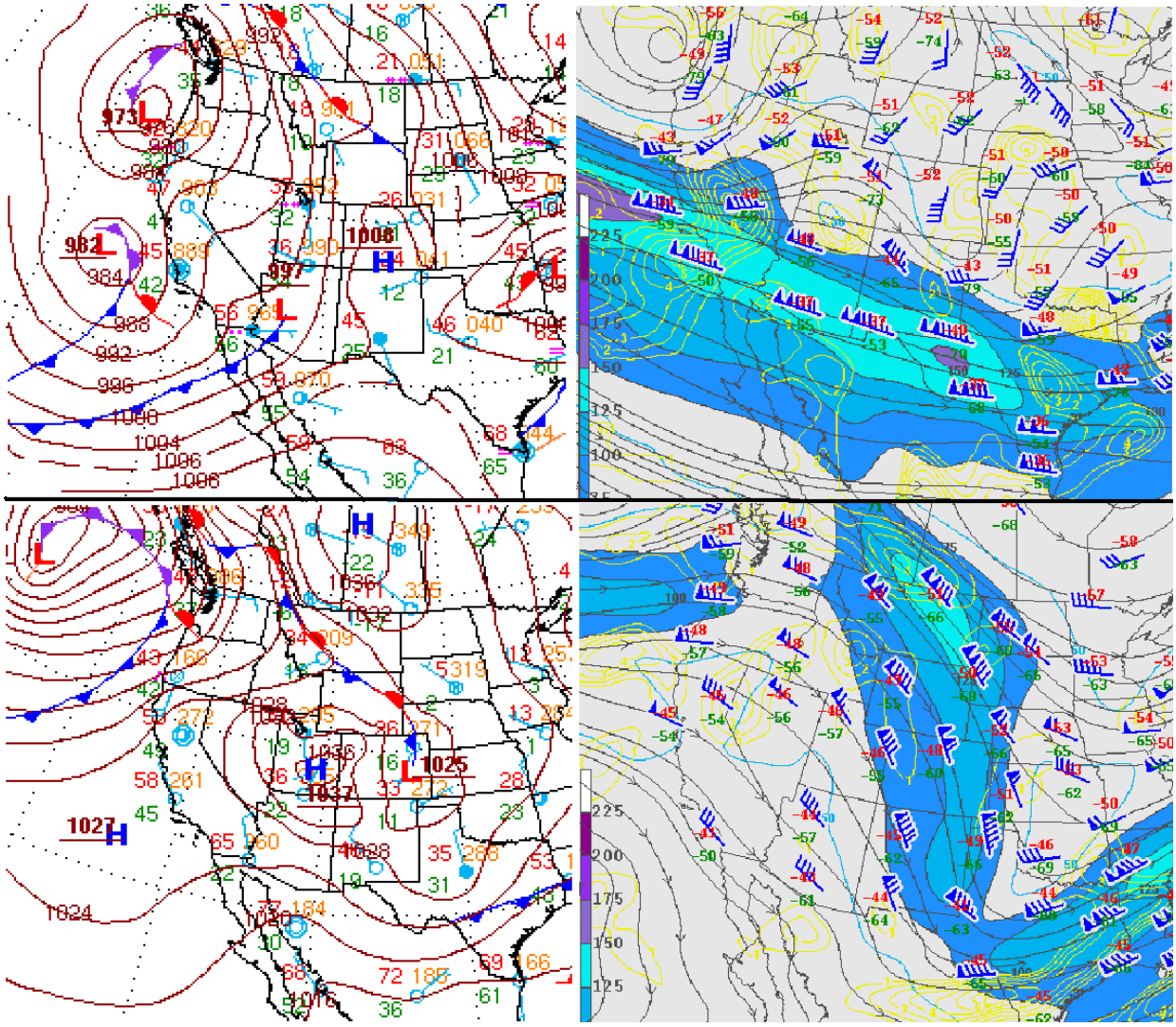

Figure 6. *Surface pressure (hPa) and frontal systems (left panels) with 300 hPa winds and heights (right panels) at 1200 UTC 21 January 2010 (top) and 0000 UTC 1 January 2010 (bottom) For the surface maps on left panels, cold fronts are indicated with blue lines, warm fronts with red lines, occluded fronts with purple lines, and isobars with brown lines every 4 hPa. The observations plotted on all panels follow standard meteorological convention for surface and upper air stations. Winds are plotted as barbs (short barb = 2.5 m/s, long barb= 5 m/s, and pennant = 25 m/s). For upper air maps on right panels, streamlines are plotted as black lines with arrows and isotachs are plotted as blue lines every 12.5 m/s with shading for wind speeds ≥ 37.5 m/s.*

Overall, the analysis indicates that average Tehachapi Pass sensitivities are weakly influenced by

the large-scale and mesoscale flow through the Pass. The fact that variable, large scale flows dominate the Tehachapi Pass region in the winter seems to generate lower average sensitivities when compared to Tehachapi Pass in the summer. This result was quite different from the warm season patterns that were characterized by significant variations in the forecast sensitivity based on time of day (Zack et al. 2010a). However, interpretation of the winter results is less certain due to the issue of low ensemble spread as discussed in Section 3.

4.2 Case Example

The output data from the ensemble of simulations provide a large volume of information about the space-time connection of atmospheric variability within the simulation domain.

For most time periods and locations, the slope of the regression line associated with the forecast metric plotted against any of the state variables was essentially zero (not shown). The R^2 value was also approximately zero indicating the variable explained none of the variance of the forecast metric at the target location.

There were a few cases for specific locations and variables that did explain a substantial amount of variance of the forecast metric. The spatial plots of R^2 (Fig. 7) and sensitivity (Fig. 8) on 0900 UTC 23 January 2010 show an example where data from all ensemble members resulted in a meaningful linear relationship. In this case, the metric variable F is the average 80-m wind speed at 0900 UTC and the IC state variable is 80-m wind speed three hours earlier.

Points labeled A (79, 106), B (81, 105) and C (51, 79) in Figures 7 and 8 show different relationships between sensitivity and R^2. Large negative sensitivity values are found near point A while large positive values are found near point B with both points showing high R^2 values (Fig. 8). On the other hand, there is an area of large negative sensitivity near point C (Fig. 7) with low R^2 (Fig. 8). The sensitivity graphs for these three grid points are presented in Figure 9.

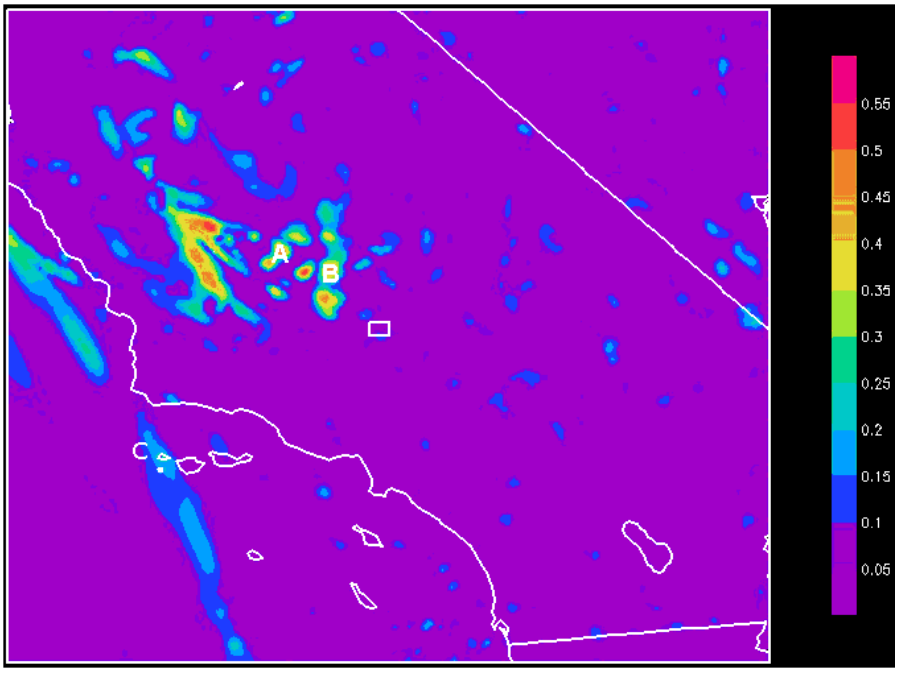

Figure 7. *Average R^2 of the 80-m wind speed in the white box at 0900 UTC 23 January 2010 to 80-m wind speed three hours earlier. Areas of high R^2 values are near points A and B and low R^2 values near point C.*

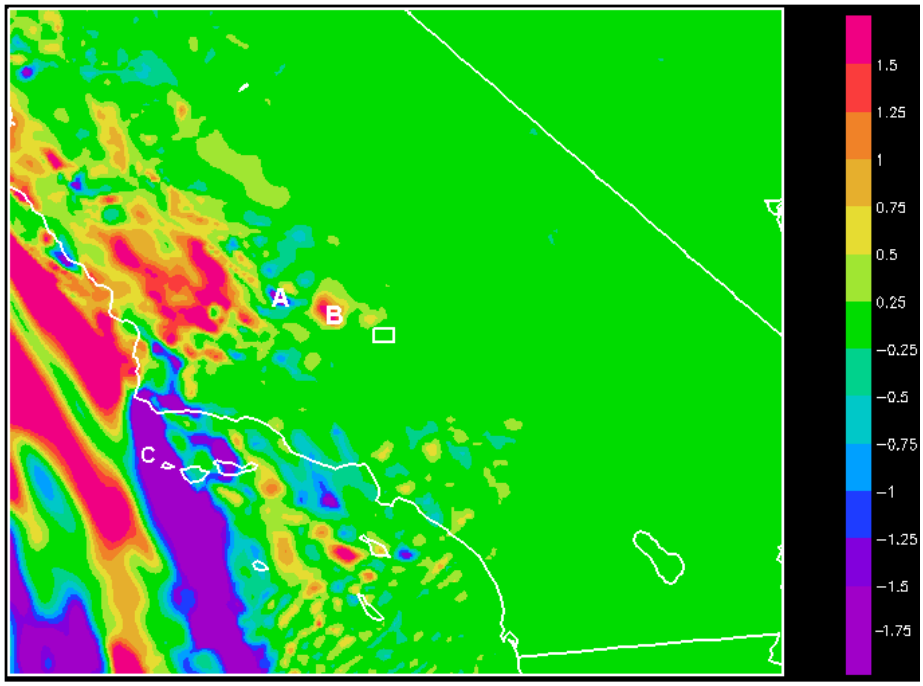

Figure 8. *The forecast sensitivity of the average 80-m wind speed in the white box at 0900 UTC 23 January 2010 to 80-m wind speed three hours earlier. Notes areas of large negative (near point A) and large positive (near point B) sensitivity both with high R^2 values (Fig. 7) and large negative sensitivity (near point C) with low R^2 values (Fig. 7).*

There is a well-defined inverse relationship at point A between changes in the 80-m wind speed IC variable and changes in average 80-m wind speed over the forecast target area three hours later (Fig. 9 left panel). The slope of the regression line at point A indicates that a 1 m/s change in 80-m wind speed is associated with a -1.8 m/s change of the 80-m wind speed in the Tehachapi Pass target area three hours later. The R^2 value for this regression is 0.43 so the variation of 80-m wind speed at 0600 UTC explains approximately 43% of the variance in the forecast target metric three hours later.

At point B, there is a well-defined direct relationship between changes in 80-m wind speed and changes in the average 80-m wind speed over the forecast target area three hours later (Fig. 9 middle panel). The slope of the regression line at point B indicates that a 1 m/s change in 80-m wind speed at point B is associated with a 1.4 m/s change of 80-m wind speed in the Tehachapi Pass target area three hours later. The R^2 value for this regression is 0.52 so the variation of 80-m wind speed at 0600 UTC explains approximately 52% of the variance in the forecast target metric three hours later. For this case, both points A and B represent areas where the ensemble produces results that can be explained well by a linear relationship. Therefore, a better estimate of the IC variable (80-m wind speed) in these locations would contribute to a predictable change in the value of the forecast metric, and can be well approximated by the linear regression shown in Figure 9.

Unlike points A and B, point C has high sensitivity but is poorly represented by the linear relationship as indicated by a low R^2 value at point C. There is an inverse relationship at point C between changes in 80-m wind speed and average 80-m wind speed over the forecast target area three hours later (Fig. 9 right panel). The slope of the regression line at point C indicates that a 1.0 m/s change in the 80-m wind speed is associated with a -3.8 m/s change of 80-m wind speed in the Tehachapi Pass target area three hours later. The R^2 value for this regression is 0.16 so the variation of 80-m wind speed at 0600 UTC explains approximately 16% of the variance in the forecast target metric three hours later. These results illustrate that although there is a high magnitude sensitivity, the linear regression explains only a small part of the wind speed variance three hours later at the metric location for point C.

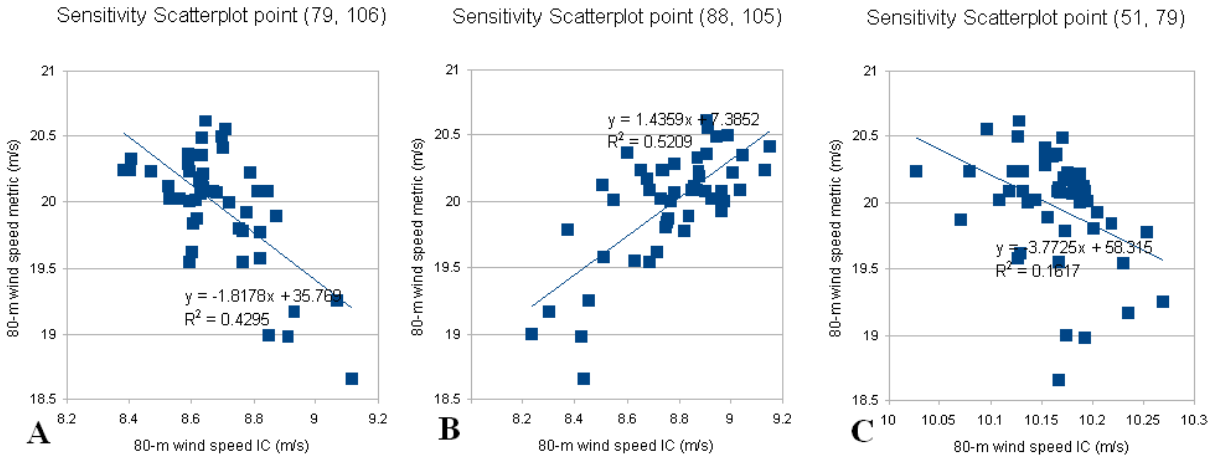

Figure 9. Scatter plot of 80-m wind speed (IC variable) for model grid points A (79, 106), B, (81, 105) and C (51, 79) at 0600 UTC 23 January 2010 versus 80-m wind speed (forecast metric) at 0900 UTC from each of the 46 ensemble members and the associated regression lines.

4.3 Climatology of Sensitivity

In order to make inferences about the best measurement locations and variables to improve forecast performance over a wide variety of cases, it is necessary to analyze a statistical composite of sensitivity values over a representative sample of cases. Two analyses were performed. One analysis included all cases (Sections 4.3.1-4.3.5) while the other was done on a subsample of cases (Section 4.3.6) that focused only on periods of higher ensemble variance as described in Section 2.

4.3.1 Look-Ahead Time Sensitivities

The average 46-day sensitivity values of 80-m wind speed in the target box to 80-m wind speed for a 1-hour look-ahead period are shown in Figure 10 (left panel). The highest sensitivity values for the 1-hour look-ahead time are in close proximity to the metric location and along the southern boundary of the grid. The 3-hour look-ahead time sensitivities are weak through most of the domain with the exception of some large values located in areas off shore in the southwest corner of the domain and near the boundaries (Fig. 10 right panel). These high values are most likely due to the variance issues discussed in Section 3.

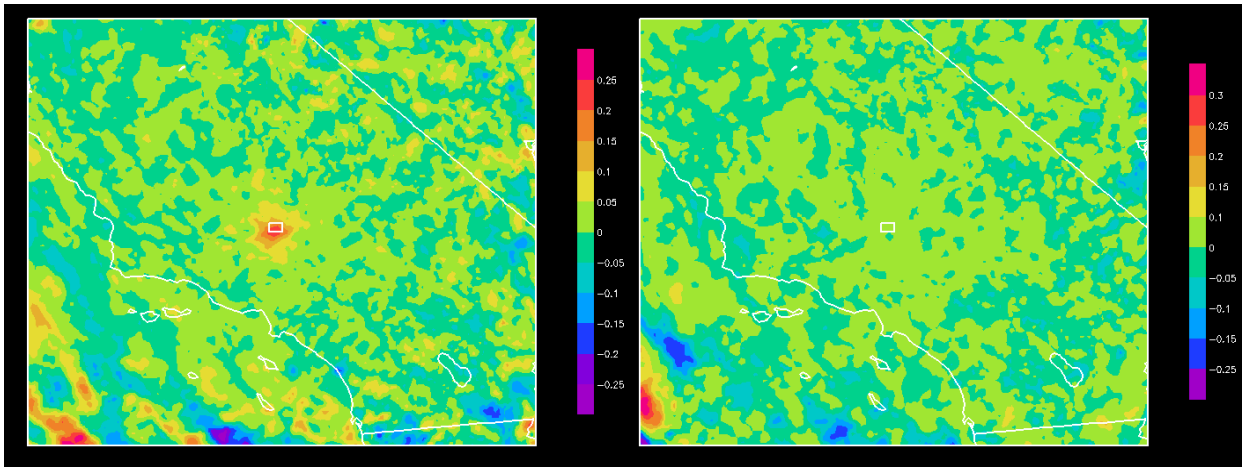

Figure 10. *Average sensitivity of 80-m wind speed (m/s) within the white target box to 80-m wind speed (m/s) throughout the entire grid domain for a 1-hour ahead (left) and 3-hour ahead (right) forecast for all time periods in the 46-day analysis period for the Tehachapi Pass Region. Note that the scale extends from -0.25 to 0.25 on the left, and -0.25 to 0.30 on the right.*

4.3.2 Sensitivity of Different IC Parameters

To determine the impact of other variables on wind speed at the target locations, the thirteen IC parameters listed in Section 2.3 were examined for all three metric locations. This subsection examines how sensitivity varies among variables.

Unlike the Tehachapi and Mid-Colombia summer season results (Zack et al. 2010a, b), 80-m winds were not clearly the best variable to predict wind speed at 80-m within the target location at a later time although it still produced somewhat higher values of R^2 when compared to other

initial condition variables. Sensitivities were also computed for 250-m AGL wind speed, 1.5-km AMSL wind speed and 3-km AMSL wind speed for the three target locations.

The wind speeds at all levels produced similar results to those from the 80-m level. Figure 11 shows that the 3-km level wind sensitivities are similar to those at 80-m (right panel of Fig. 10). A few areas of high sensitivity are located mainly over water in the southwest part of the domain. Sensitivities are weak elsewhere. The larger sensitivities in the southwest part of the domain may be due to their location near the upstream boundary and the perturbations introduced by the EnKF. Section 4.3.3 shows that R^2 values are consistently very small in this region, suggesting that none of the sensitivities have any forecast utility.

The role of wind speed change with height (i.e. wind shear) was also examined as an IC parameter for the three layers listed in Table 1 (10-m to 80-m AGL, 80-m to 500-m AGL, 500-m to 1-km AGL). The sensitivity patterns for wind shear were quite similar to those of raw wind speed at various heights, with the greatest sensitivity values located in the southwest corner of the domain. Results for the 10-m to 80-m AGL layer that is just below turbine height are shown in Figure 12.

A similar sensitivity pattern to 80-m wind was also observed for the 3-hour look-ahead time in other variables such as the 2-m surface temperatures and the 2-m to 80-m temperature difference IC parameter (Figs. 13 and 14). Sensitivity plots for other variables are provided in Appendices C and D.

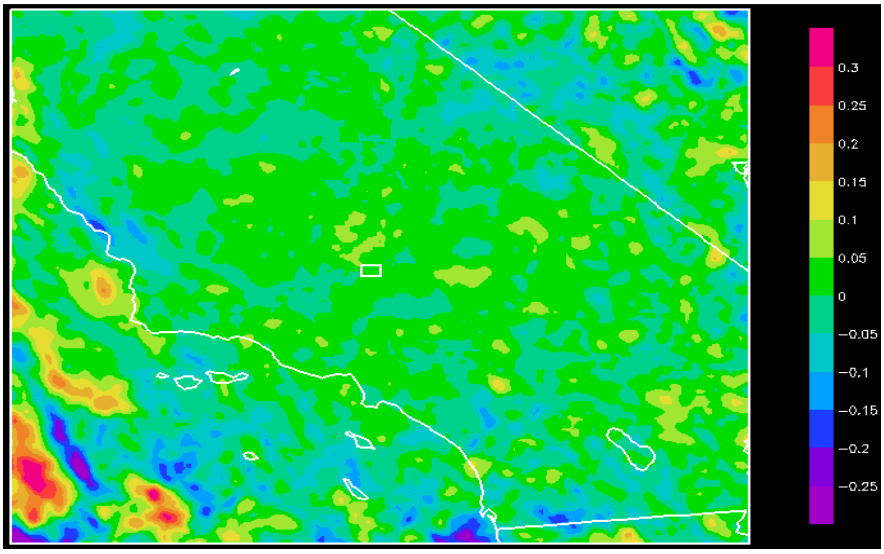

Figure 11. *Average sensitivity of 80-m wind speed (m/s) within the white target box to 3-km AMSL wind speed (m/s) throughout the entire grid domain for a 3-hour ahead forecast for all time periods in the 46-day analysis period. Note that the scale extends from -0.25 to 0.30.*

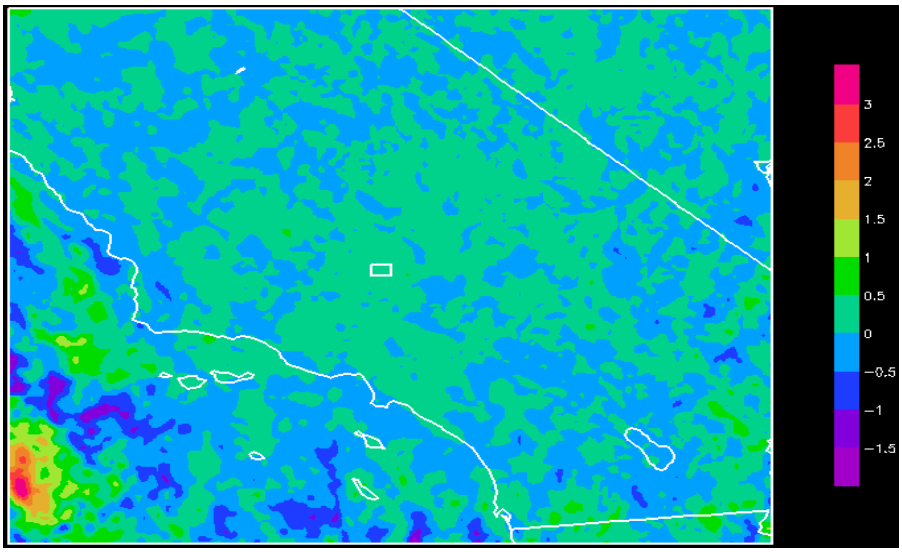

Figure 12. *Average sensitivity of 80-m wind speed (m/s) within the white target box to 10-m to 80-m AGL wind shear throughout the entire grid domain for a 3-hour ahead forecast for all time periods in the 46-day analysis period. Note that the scale extends from -1.5 to 3.0.*

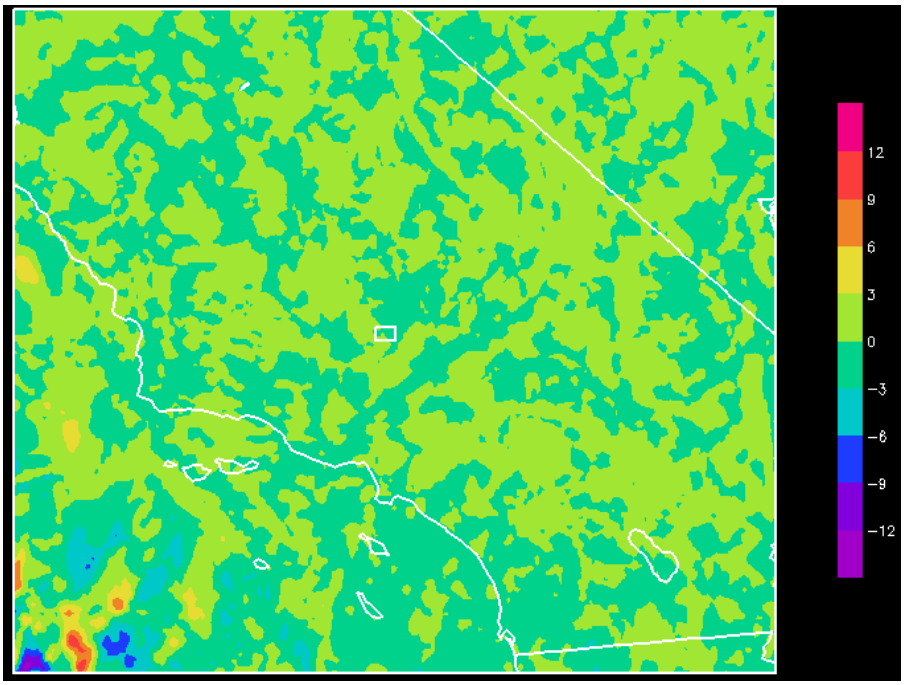

Figure 13. *Average sensitivity of 80-m wind speed (m/s) within the white target box to 2-m temperature throughout the entire grid domain for a 3-hour ahead forecast for all time periods in the 46-day analysis period. Note that the scale extends from -12 to 12.*

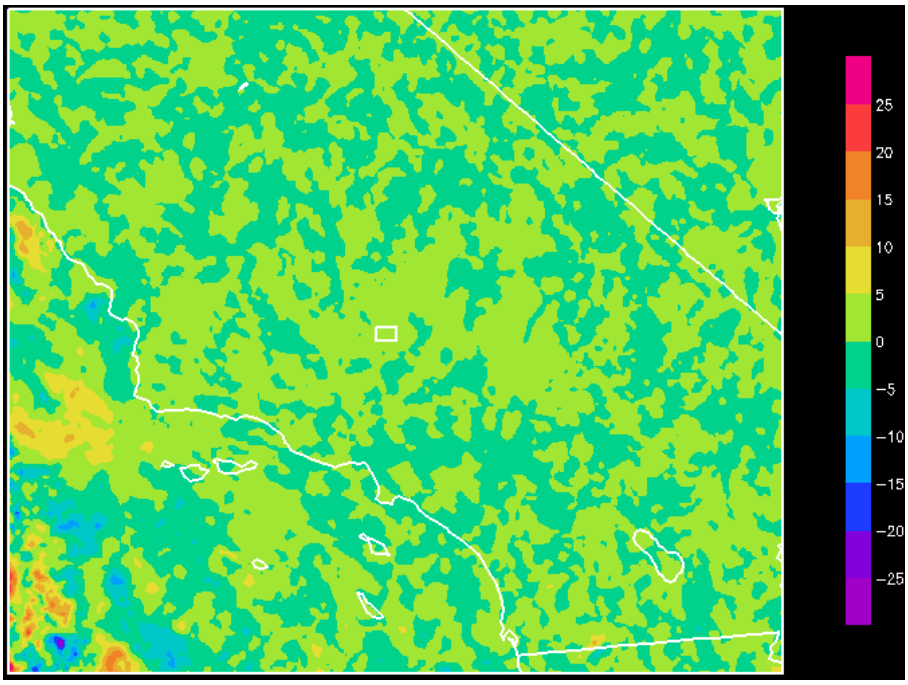

Figure 14. *Average sensitivity of 80-m wind speed (m/s) within the white target box to 2-m to 80-m temperature difference throughout the entire grid domain for a 3-hour ahead forecast for all time periods in the 46-day analysis period. Note that the scale extends from -25 to 25.*

The vertical temperature gradient sensitivities were also examined for the 80-m to 500-m AGL, 500-m to 1-km AGL, and the 80-m to 1-km AGL layers. These IC variables as well as some of the wind shear IC variables did not produce any obvious regions of high sensitivity (Appendix C). Overall, sensitivities were weak at all levels of the atmosphere for all variables.

4.3.3 Coefficient of Determination (R^2) Analysis

Similar to a map of sensitivities (e.g. Fig. 9), R^2 can be plotted for the entire region (Fig. 15) as well. The average R^2 for 80-m wind speed at every grid point for all 46 days show large values surrounding the immediate target area. Unlike the sensitivity plots, there is no region of elevated R^2 values in the southwest corner of the domain. This pattern suggests that regions of high sensitivity in the southwest part of the domain will provide no value in improving the forecast of 80-m wind speed at the target location. As discussed in the previous section for sensitivities, R^2 values decrease with increasing look-ahead hour. For all initial condition variables, the highest R^2 values are located in close proximity to the forecast metric location. Therefore initial conditions close to the forecast target location seem to have some value to the forecast of 80-m wind speed at the target location.

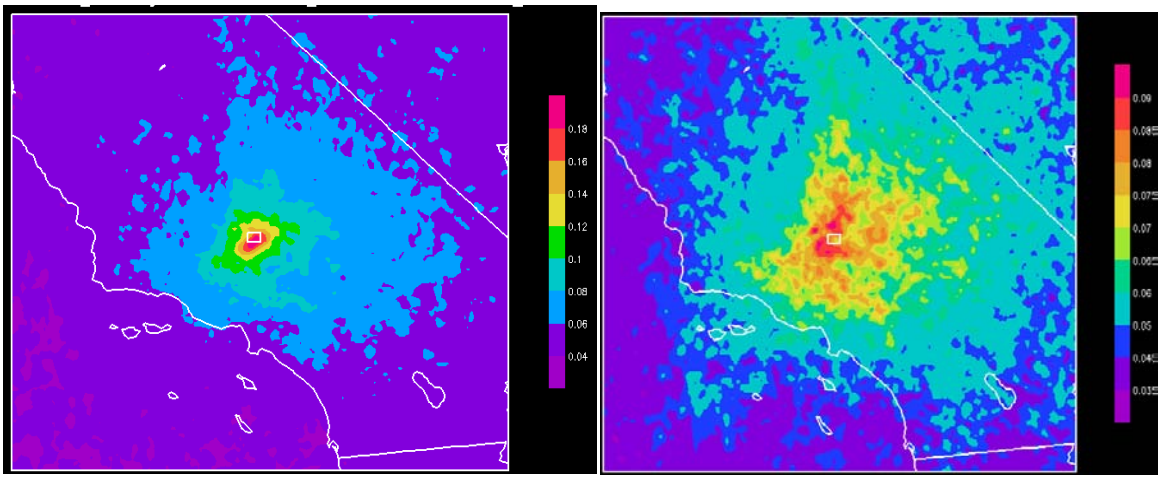

Figure 15. *Average R^2 of 80-m wind speed (m/s) within the white target box to 80-m wind speed throughout the entire grid domain for a 1-hour (left) and 3-hour (right) look-ahead period over all time periods in the 46-day analysis period. Note that the scale extends from 0.0 to 0.190 (left) and 0.0 to 0.090 (right).*

There is a notable decrease in the magnitude of R^2 with increasing look-ahead time and distance from the forecast site (Fig. 15 left and right panel comparison) similar to the changes in sensitivity (Fig. 9). The higher 1-hour look-ahead sensitivities and R^2 values for 80-m wind speed very close to the target location show that persistence tends to dominate as the best forecast method at very short lead times. Similar to the Tehachapi Pass and Mid-Columbia Basin warm season studies, as the look-ahead time increases, correlations between the IC parameter and the metric parameter tend to decrease but more significantly in this Tehachapi winter study. However, the area of highest explained variance of the regression was typically a larger circular pattern surrounding the target area at the 3-hour look-ahead periods as compared to being farther

upstream in the previous studies (Zack et al. 2010a, b).

The pattern of 3-hour R^2 values for the IC 2-m to 80-m temperature difference (Fig. 16) is similar to the one for 80-m wind speed IC (Fig. 15 right panel). The magnitude and spatial extent of the R^2 results for all other initial condition parameters were similar to those shown in Figures 15 and 16. Appendix D has R^2 plots for additional IC variables.

These results imply that the information in the initial state is most correlated near the target region. It should be noted that the structure and magnitude of the R^2 results, as well as the sensitivities, were impacted by the ensemble spread problems discussed in Section 3. So these results may not be truly representative of all uncertainty in the regional flow. Locations of maximum average R^2 presented in this section were also used to calculate a multivariate regression discussed in Section 5.

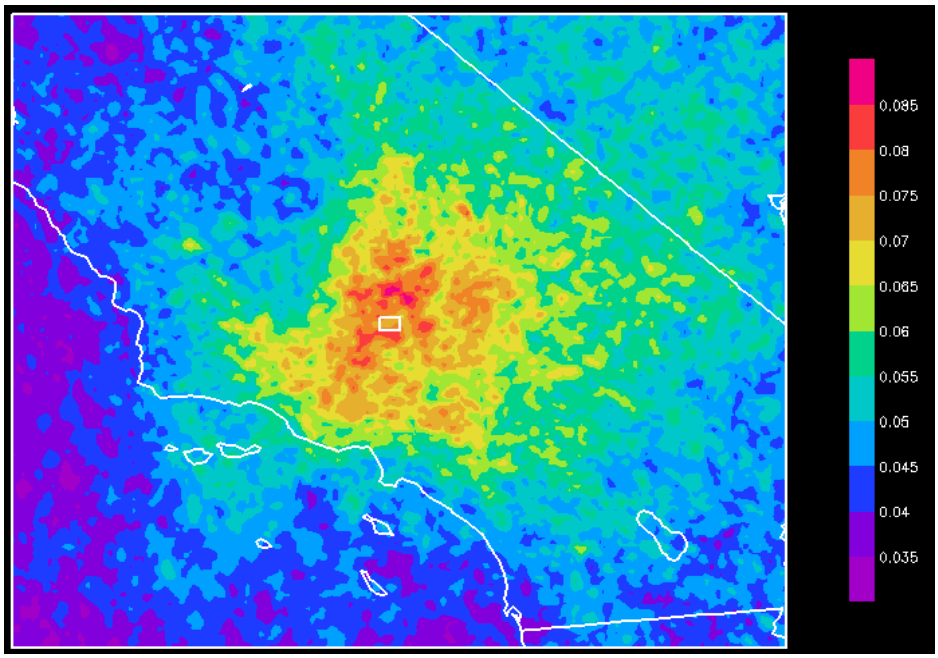

Figure 16. *Average R^2 of the sensitivity of 80-m wind speed (m/s) within the white target box for the 2-m to 80-m temperature difference throughout the entire grid domain for a 3-hour ahead forecast during all time periods in the 46-day analysis period. Note that the scale extends from 0.0 to 0.085.*

4.3.4 Significant Sensitivities

As noted earlier, an alternative summary statistic is the frequency with which an IC variable exhibits statistically significant non-zero sensitivity at the 95% confidence level. If this criterion is satisfied for a specific grid point and time, it indicates only a 5% probability that the sensitivity was produced by random data variations drawn from a sample in which the actual sensitivity was zero or of a different sign than the estimated sensitivity. Thus, it is very unlikely that the actual sensitivity is zero or of a different sign at that point and time. However, this statistic does not provide information about the magnitude of the sensitivity.

For the Tehachapi Pass region, the statistically significant non-zero sensitivity at the 95% confidence level was computed for each forecast interval in the 46-day analysis sample. Then the fraction of the 46-day sample having non-zero sensitivity was calculated for each of the IC variables under consideration. Figure 17 illustrates the frequency of statistically significant non-zero sensitivity to 80-m wind speed for a 3-hour forecast of the average 80-m wind speed in the metric area (white box).

The pattern of significant sensitivities (Fig. 17) resembles the R^2 sensitivity pattern (Fig 15 right panel), with the areas of highest significant sensitivity values surrounding the target location in a roughly circular pattern. The fact that the area near the metric box has a high frequency of statistically significant non-zero sensitivity (Fig. 17) but a somewhat smaller average sensitivity (Fig. 10 right panel) suggests that 80-m winds in the metric box have a more persistent, but smaller sensitivity to the local values 3 hours earlier. The indication is that while sensitivities to the west are stronger, they are less often statistically significant. Significant sensitivity frequency plots for additional IC variables can be found in Appendix E.

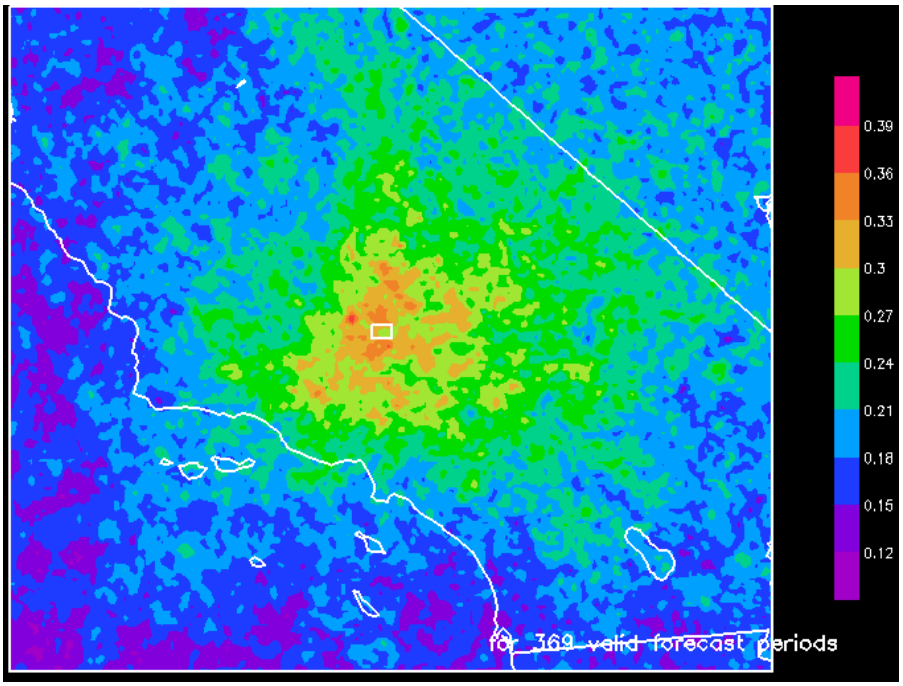

Figure 17. *Frequency (fraction of time periods) of statistically significant non-zero sensitivity at the 95% confidence level of the average 80-m wind speed in the forecast metric area (white box) to 80-m wind speed 3 hours earlier for the 46-day sample.*

4.3.5 All Case Summary

In general, the results showed weak sensitivities for all locations, variables, and levels. The area of high sensitivities that appears in the southwest corner of the domain is most likely the result of persistent southwesterly flow and an artifact of the methodology due to the interaction of the southwest flow with the boundary conditions. Further study will be needed to determine if these points are physically or just statistically correlated with the target location.

The R^2 and significant sensitivities showed similar patterns with the highest values of R^2 and significant sensitivities surrounding the target location in a quasi-circular (anisotropic) pattern. The correlation parameters, although not strong, were the largest for the (1) 80-m wind speed, (2) 250-m wind speed, (3) 2-m to 80-m temperature gradient, and (4) 10-m to 80-m wind shear. Based on these results, such parameters should provide the maximum improvements to short-range forecasts at the target locations.

4.3.6 High Variance Period Subsample

In addition to examining the full simulation period, a subsample was compiled containing just the periods with large ensemble spread in the forecast metric (referred to as the "high variance sample"). The sample was composed of 73 unique 3-hour forecast periods, as discussed in Section 2 (Table 1). For these events, the average sensitivity, average R^2, and significant sensitivities were computed for the subsample. The average sensitivities of 80-m wind speed within the white target box to 3-km AMSL wind speed for the subsample period (Fig 18) were higher than those for the full period (Fig. 11) but in an absolute sense, the subsample period sensitivities were still low.

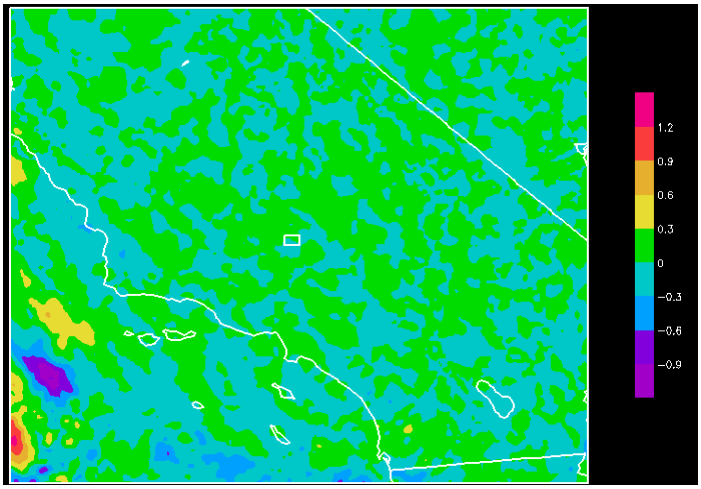

Figure 18. *Average sensitivity of 80-m wind speed (m/s) within the white target box to 3-km AMSL wind speed (m/s) throughout the entire grid domain for a 3-hour ahead forecast during the high variance subsample analysis period. Note that the scale extends from -0.9 to 1.2.*

The goal of the high variance dataset was to improve the estimates of explained variance by the linear regression for the sensitivity relationship. However, the R^2 values associated with the 80-m wind speed IC for the high variance subsample (Fig. 19) were slightly but not significantly lower than when using the full period cases (Fig. 15 right panel). These results (for the high variance subsample) showed substantial high frequency noise and a decrease in R^2 values with increasing distance away from the metric location. Results for other IC variables are shown in Appendix D. This finding was important because a major issue with the simulations was lack of ensemble spread. It was expected that days with larger metric variable spread would yield greater sensitivities, higher R^2 values, and more coherent sensitivity patterns. However, the magnitude of the metric variable spread [i.e. var(s) in Eq. 1] does not necessarily vary directly with ensemble

spread (which impacts the numerator in Eq. 1). As a result, the metric variable spread can increase leading to low R^2 values if there is no corresponding increase in ensemble spread.

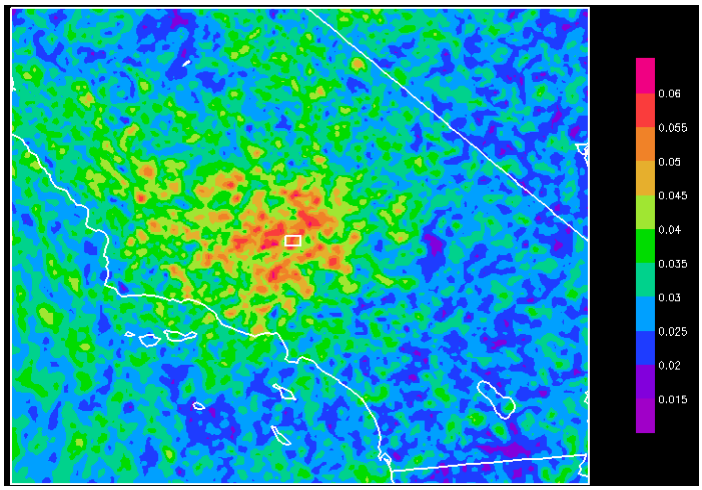

Figure 19. *Average R^2 of 80-m wind speed (m/s) within the white target box to 80-m wind speed throughout the entire grid domain for a 3-hour ahead forecast during the high variance subsample analysis period. Note that the scale extends from 0.015 to 0.060.*

5. Multiple Variable Results

Section 4 discussed the spatial variation of sensitivity and several statistical quantities used to identify the most useful locations to make measurements over the 46-day period. This section explores techniques to identify the best combination of variables and locations to achieve maximum reduction in forecast error.

MOOA was applied to the forecast sensitivity data generated for the Tehachapi Region winter season experiments. Separate calculations were performed for the full 46-day sample and a high variance subsample described in Section 2.6.

Of the thirteen variables listed in Table 1, only the (1) 80-m AGL wind speed, (2) 250-m AGL wind speed, (3) 2-m to 80-m AGL temperature difference, and (4) 10-m to 80-m AGL wind shear were chosen for use in the MOOA regression method. These four variables were selected because they showed the highest R^2.

First, the locations of the highest R^2 values were computed for all four variables at both 3-hour and 1-hour look-ahead periods (Fig. 20). For the 1-hour look-ahead results, the locations are all within the metric box indicating that off-site observations would have little beneficial use for improving a 1-hour forecast. These results highlight the importance of persistence dominating the 1-hour look-ahead period and suggest that only information within the metric region has some value. The generally low R^2 values (not shown) compared with previous studies (Zack et al. 2010a, b) indicate that these results may be impacted by the lack of ensemble variance discussed in detail in Section 3. To examine the predicted impact of more than one observation on the initial state to the simulated metric value at a later time, 1-, 2-, 3-, and 4-variable regressions were computed for both the 1- and 3-hour look-ahead period shown in Table 5.

Table 5. Average R^2 value for 1-, 2-, 3-, and 4-variable sensitivity regression for a 3-hour and 1-hour forecast of 80-m wind speed in the Tehachapi target area for all time periods.

IC Variables	All Periods 3-hour	All periods 1-hour
One Variable		
(1) 80-m wind speed	0.100	0.197
(2) 250-m wind speed	0.095	0.199
(3) 10-m to 80-m wind shear	0.093	0.166
(4) 2-m to 80-m temperature difference	0.090	0.145
Two Variables		
(1) and (2)	0.172	0.293
(1) and (3)	0.168	0.286
(1) and (4)	0.172	0.284
(2) and (3)	0.170	0.291
(2) and (4)	0.165	0.283
(3) and (4)	0.162	0.256
Three Variables		
(1), (2) and (3)	0.230	0.361
(1), (2) and (4)	0.230	0.360
(1), (3) and (4)	0.225	0.350
(2), (3) and (4)	0.225	0.352
Four Variables		
(1), (2), (3) and (4)	0.276	0.415

When comparing R^2 values for 1-, 2-, 3-, and 4-variable regressions, there is a substantial decrease from the 1- to 3-hour look-ahead period. This result suggests that the value of an observation decreases significantly with increasing look-ahead time. Three other conclusions can be drawn from the statistics shown in Table 5:

1. Each variable explains about the same amount of variance as any other variable.
2. For a given number of variables in combination, the particular combination of variables affects the R^2 value only slightly or not at all.
3. Adding a variable to any given combination increases the R^2 value significantly. The increase is nearly the same, no matter which variable is added to the combination. This result is even true when adding 250-m wind speed to a combination or single variable that includes 80-m wind speed.

For the Tehachapi winter study, any of the four variables selected is about as useful the others in providing independent information to improve forecasts. These MOOA results are significantly different than those from the Mid-Columbia or Tehachapi summer ensembles (Zack et al. 2010a, b) and are quite possibly an artifact of the unrealistically low ensemble spread.

The highest explained variance in the modeled sensitivity relationship was produced by using a 4-variable regression for both the 1- and 3-hour look-ahead period. The coefficient values for a 4-variable regression are shown in Table 6 for the 1- and 3- hour look-ahead periods. The 80-m and 250-m wind speeds have the largest coefficient for the 1-hour look-ahead period. This result suggests that persistence is the best indicator for the 1-hour look-ahead period, and 80-m wind speed at the target location is most sensitive to the initial value of these variables. This interpretation changes when looking at the 3- hour look-ahead period where 10-m to 80-m AGL wind shear has the largest coefficient value.

Table 6. Average coefficient values of the 4-variable sensitivity regression for a 3- and 1-hour forecast of 80-m wind speed in the Tehachapi target area for all time period

IC Variables	All Periods 3-hour	All Periods 1-hour
Four Variables		
(1) 80-m wind speed	0.025	0.160
(2) 250-m wind speed	0.014	0.184
(3) 10-m to 80-m wind shear	0.056	0.037
(4) 2-m to 80-m temperature difference	-0.014	-0.009

Correlations were also computed for the 3-hour look-ahead period over a high variance subsample. The general location of the highest R^2 values is all in close proximity to the target region for both the full period results and the high variance case results (Fig. 21). This finding is similar to previous results for the Mid-Columbia Basin region (Zack et al. 2010b) with the exception that the highest R^2 locations for each variable are not in one particular direction away from the metric location, but scattered in all directions close to the target location. The absence of preferred locations may be due to the highly variable nature of wind direction from case to case for the winter regime as well as the low variance in the ensemble described in Section 3.

The R^2 values for the resulting regression equations at the metric site for the 3-hour look-ahead period during both the full period and the high-variance subsample are listed in Table 7. Using all four variables, there was actually a slight decrease in R^2 from the full period to the high variance sample as opposed to the increase that was hypothesized. This trend means that the high variance period actually had less predictive value than the complete period. The implication is that low ensemble spread played only a partial role in generally low R^2 values and the assessment of uncertainty in the flow was not improved by increasing the average variance of the sample.

Even for the high-variance cases, the ensemble spread was low compared to the Tehachapi summer ensemble. This point is illustrated by the variance of 5-25 m^2/s^2 (approximate standard deviation of 2-5 m/s) within the metric box for the summer cases (Fig. 2 left panel) compared with a variance on the order of 0.25 m^2/s^2 (standard deviation around 0.5 m/s) for high-variance

winter cases (Fig. 3). With the exception of the event on 0000 UTC on January 20 (even for high-variance winter cases shown in Fig.4 top panel), the ensemble spread indicates little if any uncertainty in the phase, amplitude, or occurrence versus non-occurrence of ramping events. So, both the amount and type of ensemble spread may play a role in the low R^2 values.

The coefficient values of the 4-variable regression are shown in Table 8. For all cases, the 10-m to 80-m AGL wind shear has the largest value while the 2-m to 80-m temperature difference has the largest value for high-variance cases. However, there is much less variation in coefficient magnitude for the high-variance cases than for all cases.

Overall, the Tehachapi winter 4-variable regressions show significantly lower explained variance than the 3-variable regressions for the Mid-Columbia Basin and the Tehachapi regions during the summer (Zack et al. 2010a, b). As a result, there is some uncertainty in the findings from this study, especially due to the relative small variation of the R^2 value for a given number of variables in a combination, no matter which variables were included.

In addition to examining averages, explained variance, and coefficient values during the full 46 day period, a subsample of high-variance events was also examined. The variability of R^2 for a 4-variable regression is shown in Figure 22 for a sample of the high variance cases. Events at the beginning of the period around 10 January show the highest R^2 values ranging from 0.6 to 0.75 but quickly decrease for the rest of the period except for isolated instances on January 24 and February 7.

A similar trend shows up in the coefficient values for the 4-variable regression with higher magnitude coefficient values around 13 January (Fig. 23). The highest single event coefficient value occurs on 7 February for the 80-m wind speed variable. Overall, there is a high degree of variability from case to case for the explained variance and the 4-variable coefficient values. Specific events for 10 and 13 January as well as 7 February may have some predictive value even though most of the high variance subsample exhibits low explained variance (~0.2).

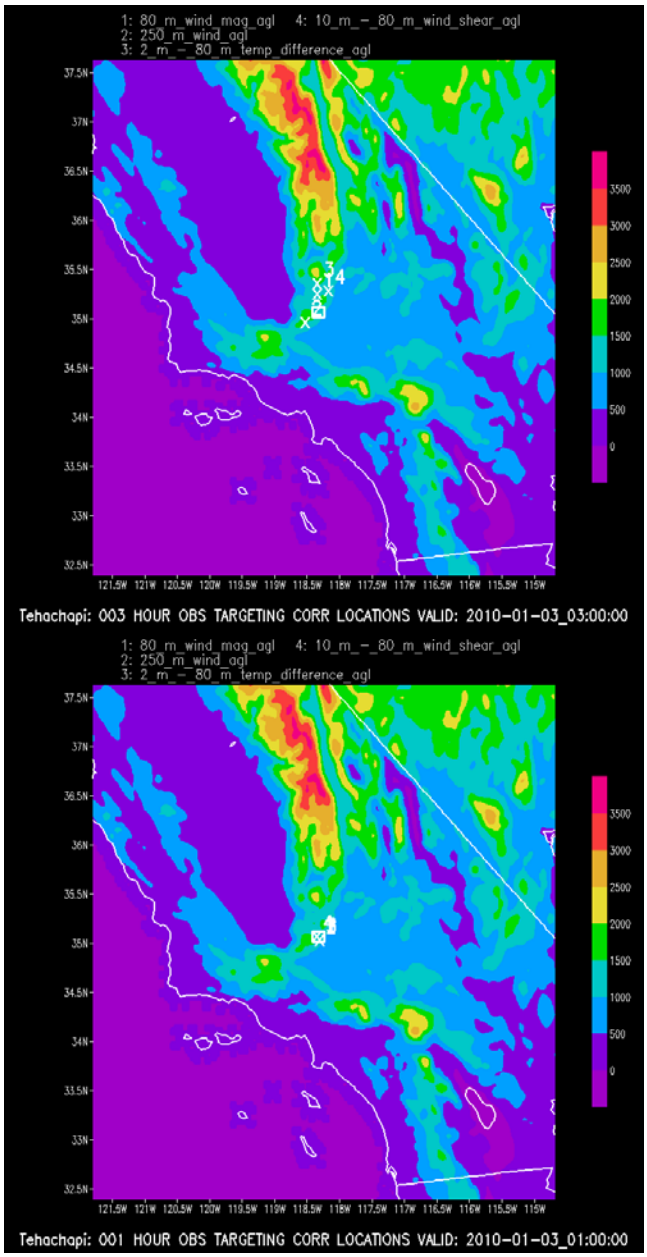

Figure 20. *Points of maximum average 46-day R^2 sensitivity for a 3-hour (top) and 1-hour (bottom) forecast of the average 80-m wind speed over the Tehachapi target area (white box) for four IC variables: (1) 80-m wind speed, (2) 250-m wind speed, (3) 10-m to 80-m wind shear, and (4) 2-m to 80-m temperature difference. The color shading depicts the elevation (m) of the model terrain above sea level.*

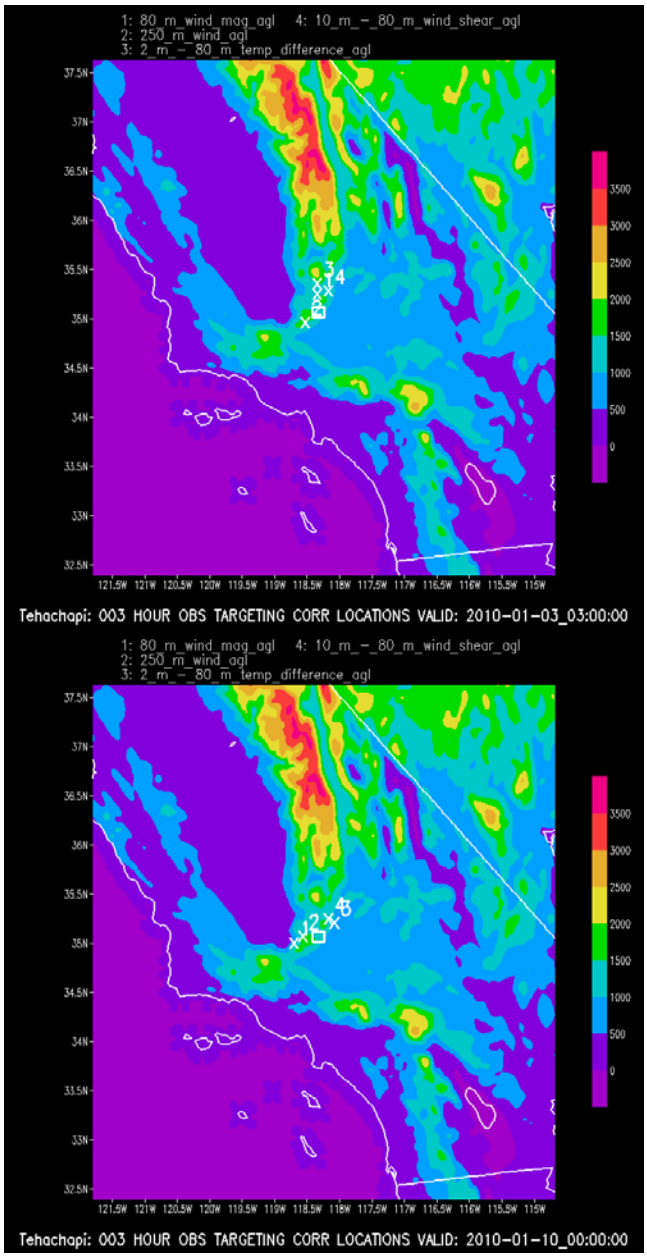

Figure 21. *Points of maximum average 46-day (top) and high variance subset (bottom) R^2 sensitivity for a 3-hour forecast of the average 80-m wind speed over the Tehachapi target area (white box) for four IC variables: (1) 80-m wind speed, (2) 250-m wind speed, (3) 10-m to 80-m wind shear, and (4) 2-m to 80-m temperature difference. The color shading depicts the elevation (m) of the model terrain above sea level.*

Table 7. Average R^2 value for 1-, 2-, 3-, and 4-variable sensitivity regression for a 3-hour forecast of 80-m wind speed in the Tehachapi target area for all time periods and high-variance periods.

IC Variables	All Periods 3-hour	High-Variance Periods 3-hour
One Variable		
(1) 80-m wind speed	0.100	0.067
(2) 250-m wind speed	0.095	0.069
(3) 10-m to 80-m wind shear	0.093	0.072
(4) 2-m to 80-m temperature difference	0.090	0.073
Two Variables		
(1) and (2)	0.172	0.125
(1) and (3)	0.168	0.129
(1) and (4)	0.172	0.131
(2) and (3)	0.170	0.127
(2) and (4)	0.165	0.131
(3) and (4)	0.162	0.122
Three Variables		
(1), (2) and (3)	0.230	0.179
(1), (2) and (4)	0.230	0.181
(1), (3) and (4)	0.225	0.18
(2), (3) and (4)	0.225	0.171
Four Variables		
(1), (2), (3) and (4)	0.276	0.220

Table 8. Average coefficient values of the 4-variable sensitivity regression for a 3-hour forecast of 80-m wind speed in the Tehachapi target area for all time periods and the high-variance periods.

IC Variables	All Periods	High-Variance Periods
Four Variables		
(1) 80-m wind speed	0.025	0.035
(2) 250-m wind speed	0.014	0.026
(3) 10-m to 80-m wind shear	0.056	0.027
(4) 2-m to 80-m temperature difference	-0.014	-0.048

The MOOA analysis suggests that it is necessary to utilize all four of the identified variables/locations in order to achieve consistent values for the ramp event cases during the Tehachapi winter study. However, there is likely more information to be extracted from the sensitivity dataset, given that several factors were not considered in this preliminary analysis. The results also show a significant decrease in R^2 value from previous studies (Zack et al. 2010a, b) that may be due to the lack of ensemble spread (as discussed in Section 3). The lack of improvement in the R^2 results for the high variance subset suggests other factors including that the ensemble design could not fully assess uncertainty in the winter regime.

In this study, the locations of the second, third, and fourth variables were chosen based on the maximum single variable regression R^2 value. However, the locations of maximum R^2 for each variable are not necessarily the locations that will achieve the highest R^2 for a 2- or 3- or 4-variable regression. It is certainly possible that the maximum R^2 locations may be more strongly correlated with each other than other sites with somewhat lower R^2. In this case, it is conceivable that a combination of two, three or four sites, several with R^2 values less than the maximum for single variable regression, will produce the highest R^2 value for multivariable regression. It is also possible that the best multivariable combination may include multiple occurrences of the same variable observed at two more different locations.

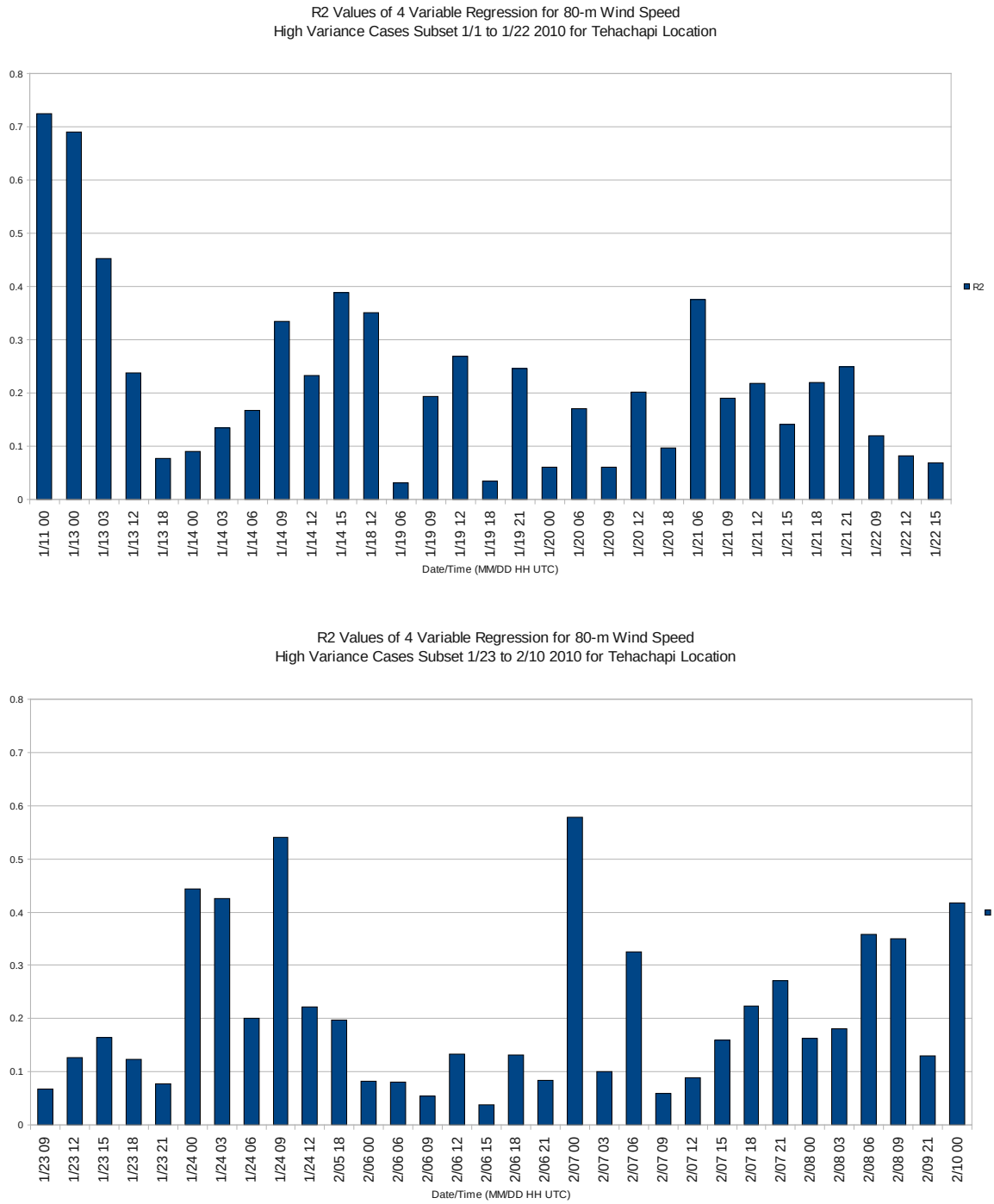

Figure 22. *A representative sample of R^2 values for a multiple regression of four normalized IC variables from their respective points of maximum average R^2 values. The R^2 values were calculated from the high variance cases listed in Table 2 for a 3-hour forecast of the average 80-m wind speed in the Tehachapi metric box.*

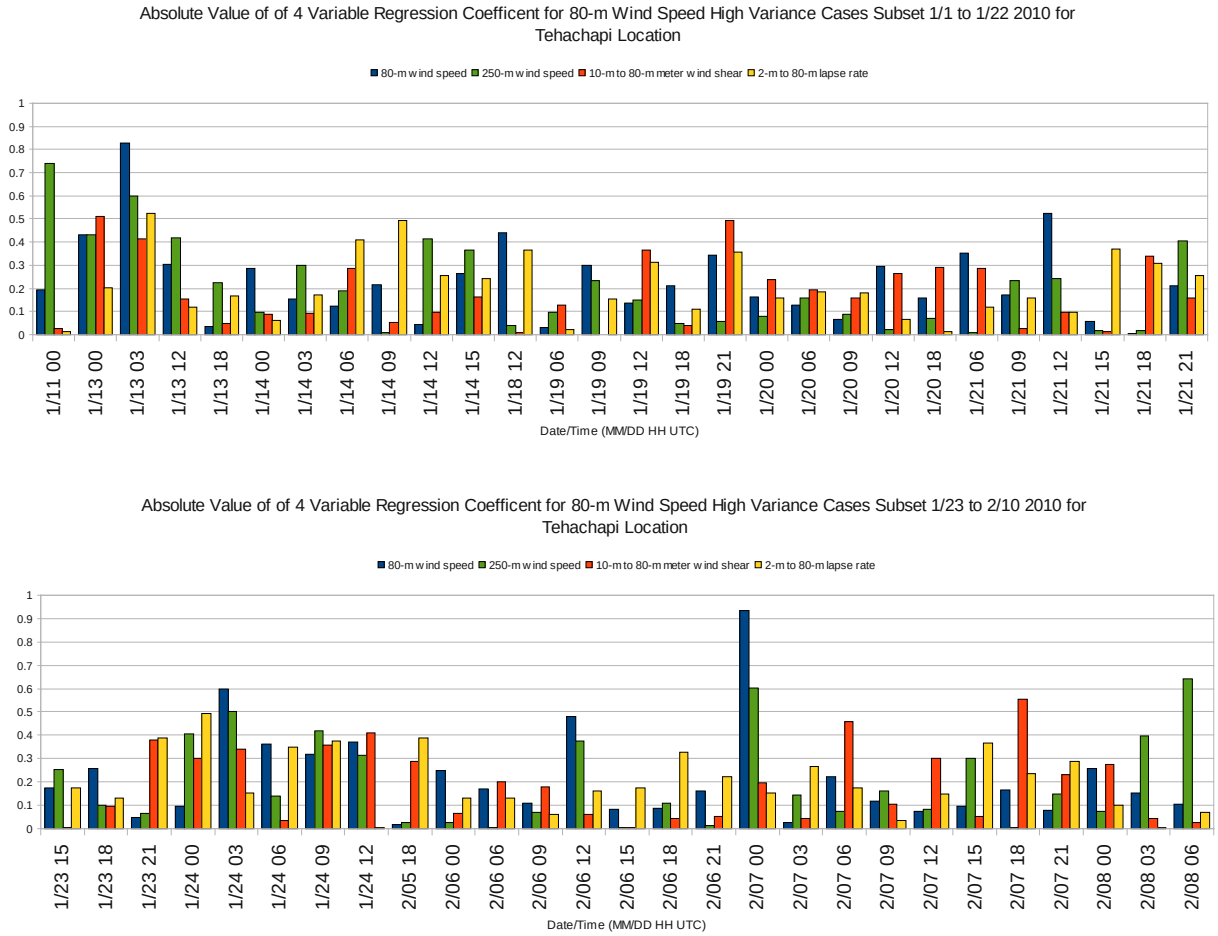

Figure 23. *A representative sample of the absolute value of the regression coefficient for combinations of four normalized IC variables from their respective points of maximum average ramp case R^2 values. The R^2 values were calculated from the high variance cases listed in Table 2 for 3-hour forecasts of 80-m wind speed in the Tehachapi metric box.*

One method to test a larger set of variables and locations would be to start with the location of highest R^2 for a single variable. A 2-variable regression could be performed with this point and every grid point for the second variable. A map of the 2-variable regression R^2 values could then be created to select a location that produces the maximum 2-variable R^2. A 3-variable regression could be performed for these two variables and locations as well as every grid point location of the third variable followed by the extraction of a second R^2 map. Finally, the location that produced the maximum 3-variable regression R^2 could be selected. Although this exercise is computationally intensive, it could be used to determine the optimal location for additional observations given a known first location and variable.

6. Summary

In past research, the ensemble sensitivity analysis (ESA) has been applied to large-scale weather prediction. Zack et al. (2010a, b) extended the ESA method to the mesoscale by adding a multiple observation optimization algorithm (MOOA) to analyze forecast sensitivity in both the Tehachapi Pass and the Mid-Columbia Basin regions in the summer season. In this current study, the ESA-MOOA approach was used to study forecast sensitivities of 80-m wind speed for a winter regime for the Tehachapi Pass region.

The ESA-MOOA is based on statistical analysis of data from an ensemble of NWP model simulations for an analysis period that is representative of the weather regimes in the area of interest. The ensemble members differ from each other due to perturbations introduced in the initial and boundary conditions of the simulations. The resulting analyses are used to estimate forecast sensitivity to prior values of atmospheric state variables for selected variables and look-ahead periods. One or more composites (e.g. averages, frequency) of forecast sensitivity parameters can then be generated to provide information about the climatological sensitivity patterns. These composite patterns can in turn provide guidance on where to deploy meteorological sensors to achieve the greatest impact on forecast performance for the desired variable and look-ahead period.

For this study the ESA-MOOA method was applied to the Tehachapi Pass during winter using the WRF 2.2 atmospheric model and DART data assimilation software. An ensemble of 48 members was generated over a period extending from 1 January to 18 February 2010. The first two days were considered to be a spin-up period for the ensemble and were excluded from the forecast sensitivity calculations. Output was saved every hour and the forecast sensitivity for 1- to 3-hour look-ahead periods was computed from the hourly output data. Thirteen prior state variables were considered in the analysis.

The initial analysis of results for the Tehachapi winter study showed noisy and widely scattered sensitivity values along with low R^2 and significant sensitivity frequency values. Further examination revealed that the ensemble suffered from extremely low spread when compared to forecasts from previous ESA-MOOA studies done for the Tehachapi and Mid Columbia summer experiments (Zack et al. 2010a, b). The Tehachapi winter results that exhibited a low ensemble spread were likely caused by an increase in the spatial correlation of the perturbations of the boundary conditions, the lack of a nested and large domain, and/or changes in the characteristic uncertainty of the seasonal flow within the region.

The 1- and 3-hour R^2 results showed persistence contributed to most of the explained variance in the forecasted metric value. Using the location of maximum 46-day average R^2 values of the sensitivity, a 4-variable sensitivity regression was computed using 80-m wind speed, 250-m wind speed, 10 to 80-m wind shear and, 2-m to 80-m temperature difference. For these variables, the highest R^2 values were associated with the 1-hour look-ahead time period and decreased with increasing look-ahead time.

Several insights can be made in comparing the Tehachapi summer and winter results. The Tehachapi summer runs (Zack et al. 2010a) had the same domain and nesting configuration as the winter runs. However, the spatial extent of perturbations in the summer runs was smaller. The regime flow was uncertain enough at the scale of these perturbations leading to significant

metric spread for the summer runs and meaningful sensitivity results. Several ideas are proposed for future ensemble experiments.

- The domain must be large enough that the extent of the boundaries is equal to the scale of the flow that contributes to forecast divergence when perturbed. It might be helpful then to run a nested grid for all domains so that the boundaries are located far from the forecast metric location. The adverse effects of covariance inflation would be mitigated by boundaries that are located away from an inner nest where observations are assimilated. When perturbed boundaries are within ~300 km (based on the current radius of influence) of observations, covariance inflation could cause the ensemble to become unstable.
- It is important to have a balance between perturbation size and magnitude so that the perturbations accurately assess the uncertainty in the initial and boundary conditions.
- It can be seen that the perturbations added little if any phase differences to the ramping events in Tehachapi Pass. It might be valuable to explore a perturbation method that introduces phase uncertainty into the ensemble (Torn et al. 2006).

The Mid-Columbia summer simulations (Zack et al. 2010b) used the same perturbation method but had a different grid nesting configuration when compared to the Tehachapi winter simulations. The Mid-Columbia summer simulations had a coarse outer and high-resolution inner nested grid and the Tehachapi winter simulations only had one high resolution grid. A comparison of the Tehachapi winter with the Mid Columbia summer experiment revealed the importance of the model nesting configuration, even with the use of identical perturbation methods. Since the perturbations for the Mid-Columbia ensemble were introduced into the outer grid, they were significantly farther from the area of interest than the perturbations introduced in the Tehachapi winter ensemble. This would imply that perturbation distance from the target location is also important in influencing the amount of forecast ensemble spread at the target location.

The results indicate that the growth, decay, and influence of perturbations on the metric variable are sensitive to the following factors.

- Amplitude and spatial extent of the perturbations must be large enough to induce spread in both the first set of initial conditions and the boundary conditions for every forecast interval.
- Type of weather regime simulated must have enough sensitivity that solutions can diverge as they respond to the perturbations.
- Model configuration parameters such as the grid nesting allow or prevent growth of the perturbation with time.

Some combination of these factors is the most likely cause of the low ensemble spread in the Tehachapi winter regime as compared to the summer season experiments.

Examination of high ensemble variance during a subsample period was performed to see if the results would change. The analysis did not reveal any regions of higher magnitude sensitivity values, higher explained variance (R^2), or increased frequency of the significant sensitivity throughout the domain for all variables. This result indicates that even though the variance was larger for the metric variable during these events, the spatial extent of variance among the initial

condition variables was not high enough to create a discernible signal/relationship.

The results of this study indicate that both the seasonal weather regimes and exact implementation of the techniques of the ESA-MOOA method have a dramatic influence on the usefulness of the results as guidance for the design of sensor networks intended to improve forecast performance. There are a number of possibilities for extending the work done in this and related studies.

- Reexamine the Tehachapi region using various techniques to introduce perturbations into the simulations and determine if low ensemble spread and sensitivities were intrinsic to the winter weather regimes or were an artifact of the implementation of the ESA-MOAA technique in this study.
- Validate forecast sensitivity and other computed fields as well as observation deployment strategies derived from them. Such validation is essential before using the methodology as a routine tool to formulate sensor network deployment strategies. These issues could be addressed by observation denial experiments using actual data gathered at target locations or observing system simulation experiments (OSSEs; Kalnay et al. 1985; Arnold and Dey 1986). Data denial and/or OSSEs would reveal whether the highly sensitive areas do indeed have a significant impact on the prediction of 80-m wind speed at target locations.
- Perform an analysis that stratifies the simulation experiments by events or weather regimes to determine the value of observations for critical events. Regime-based analysis could help determine where observations might be needed in regions that are sensitive to highly variable flows instead of focusing on the most common patterns. This regime based sensitivity analysis could also offer insight into the predictability and scales of uncertainty in various weather regimes. Regimes should be studied in concert with the perturbation technique discussed in the first bullet point.
- Conduct experiments over a longer time period to account for biases related to season and current weather regime as well as address issues of representativeness given the limited sample size.
- Expand the MOOA technique to include more variables and more target locations. This effort would help determine if there are other variables that could provide useful observation targeting information and also determine how the target sensitivity patterns change over a region and not just a few points.

7. Acknowledgements

This work performed under the auspices of the U.S. Department of Energy by Lawrence Livermore National Laboratory under Contract DE-AC52-07NA27344. The work of the authors from AWS Truepower was performed under subcontract B584259 from Lawrence Livermore National Laboratory.

8. References

Ancell, B. and G. J. Hakim, 2007: Comparing adjoint- and ensemble-sensitivity analysis with applications to observation targeting. *Mon. Wea. Rev.*, **135**, 4117-4134.

Anderson, J. L., 2001: An ensemble adjustment Kalman filter for data assimilation. *Mon. Wea. Rev.*, **129**, 2884-2903.

Anderson, J. L., T. Hoar, K. Raeder, H. Liu, N. Collins, R. Torn, and A. F. Arellano, 2009: The Data Assimilation Research Testbed: A community data assimilation facility. *Bull. Amer. Meteor. Soc.*, **90**, 1283-1296.

Evensen, G., 2007: Data assimilation: The ensemble Kalman filter, Springer, Berlin, 307 pp.

Houtekamer P. and H. L. Mitchell, 1998: Data assimilation using an ensemble Kalman filter technique, *Mon. Wea. Rev.*, **126**. 796-811.

Monteverdi, J., and J. Null, 1997: El Niño and California Precipitation. NWS Western Region Technical Attachment, No. 97-37.

Skamarock, W. C., J. B. Klemp, J. Dudhia, D. O. Gill, D. M. Barker, W. Wang, and J. G. Powers, 2005: A Description of the Advanced Research WRF Version 2, NCAR TECHNICAL NOTE: NCAR/TN–468+STR, National Center for Atmospheric Research, Boulder, Colorado, USA.

Torn, R. D., and G. J. Hakim, 2008: Ensemble-based sensitivity analysis. *Mon. Wea. Rev.*, **136**, 663-677.

Torn, R. D., and G. J. Hakim, C. Snyder, 2006: Boundary conditions for limited-area ensemble Kalman filters. *Mon. Wea. Rev.*, **134**, 2490-2502.

Zack, J., E. Natenberg, S. Young, J. Manobianco, and C. Kamath, 2010a: Application of ensemble sensitivity analysis to observation targeting for short-term wind speed forecasting. Technical Report LLNL-TR-424442, 32 pp., Lawrence Livermore National Laboratory, Livermore, CA.

Zack, J., E. Natenberg, S. Young, G. Van Knowe, K. Waight, J. Manobianco, and C. Kamath, 2010b: Application of ensemble sensitivity analysis to observation targeting for short-term wind speed forecasting in the Washington - Oregon Region. Technical Report LLNL-TR-458086, 65 pp., Lawrence Livermore National Laboratory, Livermore, CA.

Appendix A: Specifications of the ESA Configuration

Table A-1. Configuration of the WRF 2.2 model and grid used in this investigation

Grid

- Matrix Size (NX,NY,NZ): 200 X 200 X 40
- Grid cell size: ~ 4 km

Model Configuration

- WRF single-moment (WSM) 3-class ice scheme
- Long wave radiation scheme: Rapid radiative transfer model
- Short wave radiation scheme: Dudhia scheme
- Boundary layer scheme: YSU scheme
- No convective parameterization
- 60 second time step on outer grid, 20-second time step on inner grid
- Runge-Kutta 3rd order time integration
- Horizontal Smagorinsky 1st order closure
- 6th-order numerical diffusion turned on

Table A-2. Configuration of the Data Assimilation Research Testbed (DART) module

- Square root Ensemble Kalman Filter
- Cycled every 6 hours 4 times a day with various observations
- Ensemble size: 48 members
- Perturbed IC from National Weather Service (NWS) Rapid Update Cycle (RUC) for first cycle
- Perturbed boundary conditions for each assimilation period, boundary conditions also from RUC
- Deterministic inflation based on spatially-varying state space (I.e. covariance inflation)
- Initial inflation standard deviation 0.6
- Initial inflation 1.0

Table A-3. Data Assimilated Every 6 Hours into the Ensemble of Simulations

Assimilated Observations	Evaluated observations
'RADIOSONDE_TEMPERATURE',	'METAR_TEMPERATURE_2_METER',
'RADIOSONDE_U_WIND_COMPONENT',	'METAR_U_10_METER_WIND',
'RADIOSONDE_V_WIND_COMPONENT',	'METAR_V_10_METER_WIND',
'RADIOSONDE_SPECIFIC_HUMIDITY',	'MARINE_SFC_U_WIND_COMPONENT',
'ACARS_TEMPERATURE',	'MARINE_SFC_V_WIND_COMPONENT',
'ACARS_U_WIND_COMPONENT',	'LAND_SFC_U_WIND_COMPONENT',
'ACARS_V_WIND_COMPONENT',	'LAND_SFC_V_WIND_COMPONENT',
'ACARS_SPECIFIC_HUMIDITY',	'DEW_POINT_2_METER',/
'MARINE_SFC_TEMPERATURE',	'LAND_SFC_TEMPERATURE',
'MARINE_SFC_SPECIFIC_HUMIDITY',	'LAND_SFC_SPECIFIC_HUMIDITY',
'RADIOSONDE_SURFACE_ALTIMETER',	
'MARINE_SFC_ALTIMETER',	
'LAND_SFC_ALTIMETER',	

Appendix B: Vertical Levels of the Model

Table C1. Approximate pressure and altitude for each model level interface for a grid point at sea level.

Model Level Number	Pressure Level pa	Approx. Altitude (m)	Model Level Number	Pressure Level pa	Approx. Altitude (m)
1	101344	0	21	34600	8250
2	100650	55	22	31900	8800
3	99700	135	23	29400	9350
4	98400	250	24	27000	9900
5	96900	375	25	24800	10,500
6	95000	550	26	22700	11,050
7	92600	750	27	20700	11600
8	89800	1000	28	18900	12,200
9	83900	1550	29	17200	12,800
10	78400	2100	30	15600	13400
11	73100	2700	31	14200	14,050
12	68200	3200	32	12800	14,700
13	63500	3800	33	11500	15,350
14	59100	4300	34	10400	16,000
15	54900	4900	35	9300	16,700
16	51000	5500	36	8300	17,450
17	47300	6000	37	7400	18,200
18	43800	6600	38	6500	18,950
19	40600	7100	39	5700	19,800
20	37500	7700	40	5000	20,600

Appendix C: Additional Variable Sensitivity Results

1-Hour Ahead

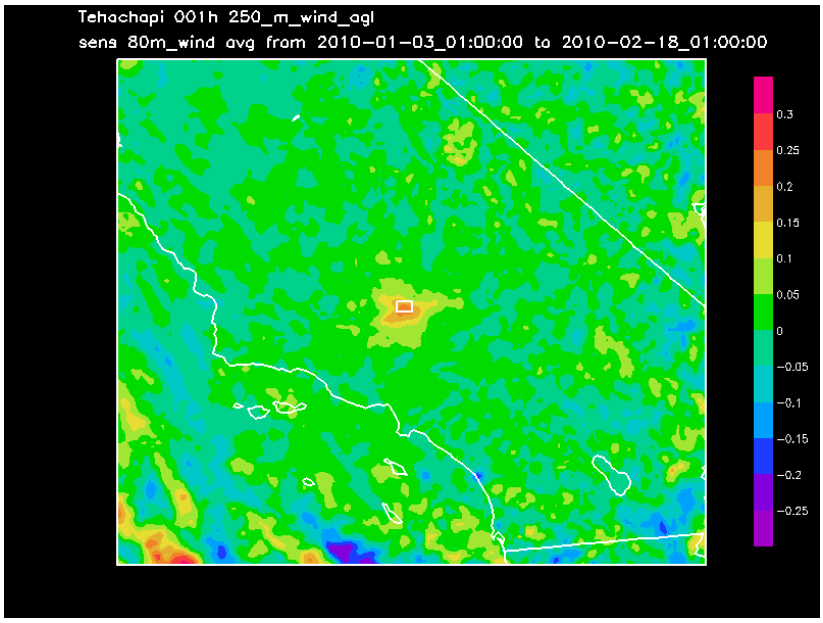

Figure C1. *Average sensitivity of 80-m wind speed (m/s) within the white target box to 250-m AGL wind speed (m/s) throughout the entire grid domain for a 1-hour ahead forecast during all time periods in the 46-day analysis period for Tehachapi.*

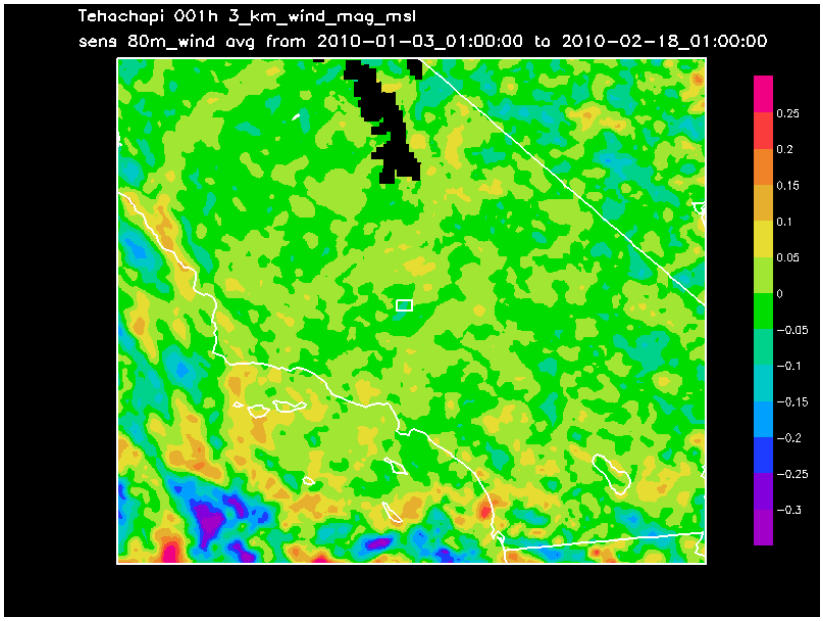

Figure C2. *Average sensitivity of 80-m wind speed (m/s) within the white target box to 3-km MSL wind speed (m/s) throughout the entire grid domain for a 1-hour ahead forecast during all time periods in the 46-day analysis period for Tehachapi.*

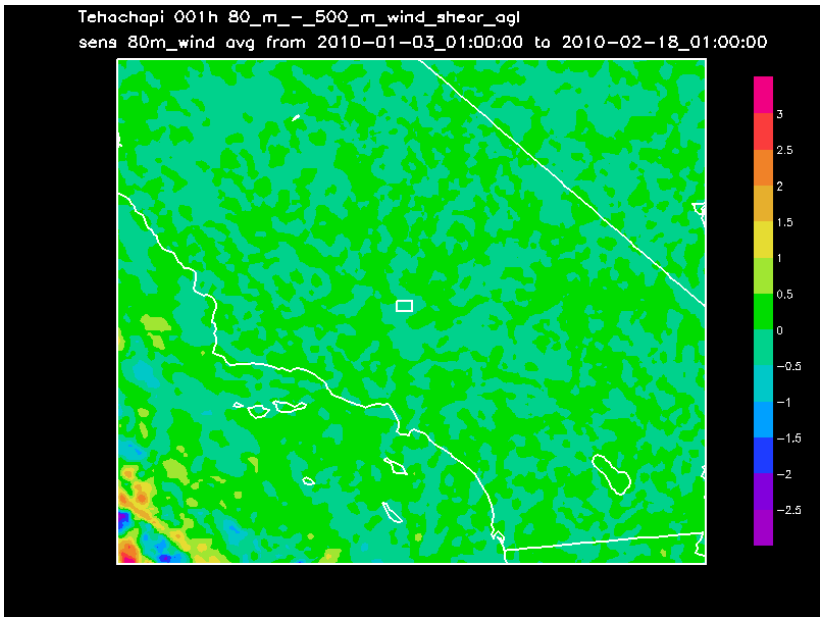

Figure C3. *Average sensitivity of 80-m wind speed (m/s) within the white target box to 80-m to 500-m AGL wind shear throughout the entire grid domain for a 1-hour ahead forecast during all time periods in the 46-day analysis period for Tehachapi.*

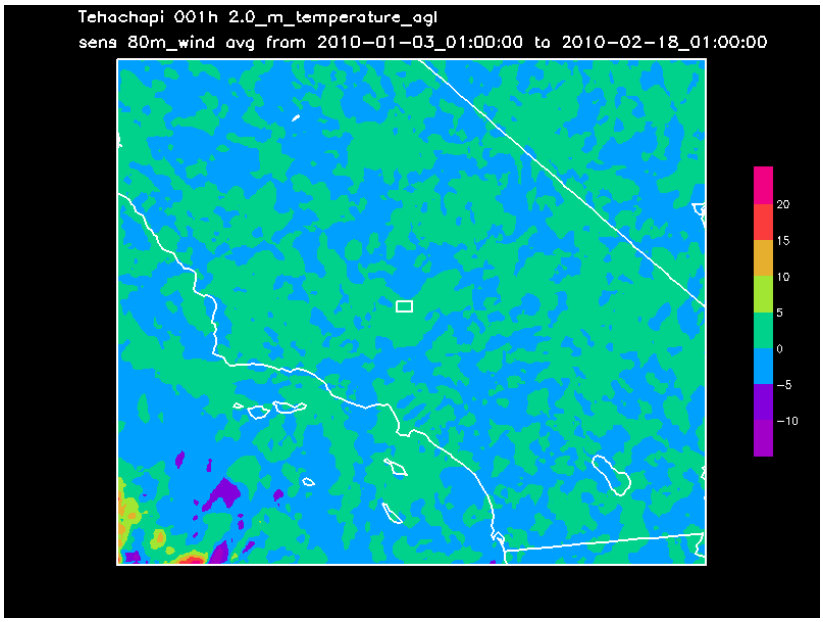

Figure C4. *Average sensitivity of 80-m wind speed (m/s) within the white target box to 80-m to 2-m AGL temperature throughout the entire grid domain for a 1-hour ahead forecast during all time periods in the 46-day analysis period for Tehachapi.*

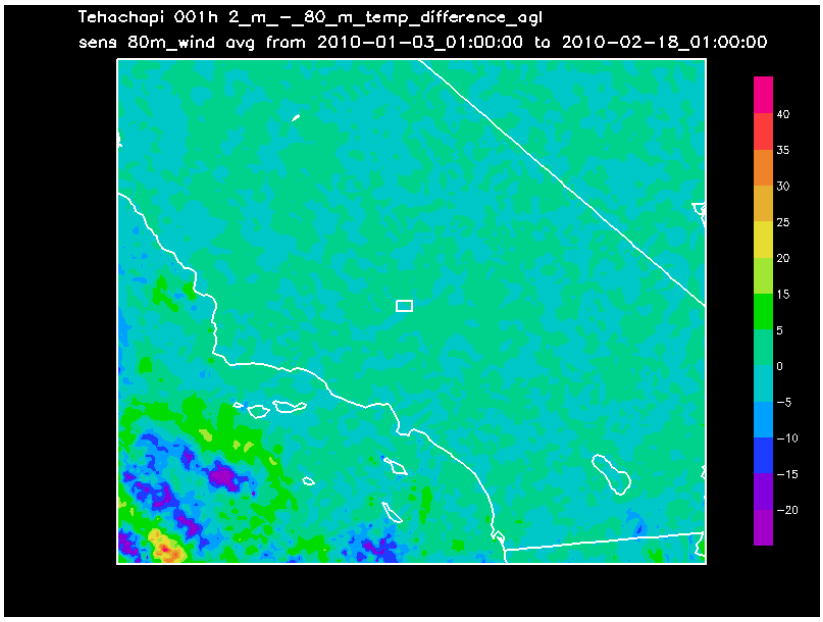

Figure C5. *Average sensitivity of 80-m wind speed (m/s) within the white target box to 2-m to 80-m AGL temperature difference throughout the entire grid domain for a 1-hour ahead forecast during all time periods in the 46-day analysis period for Tehachapi.*

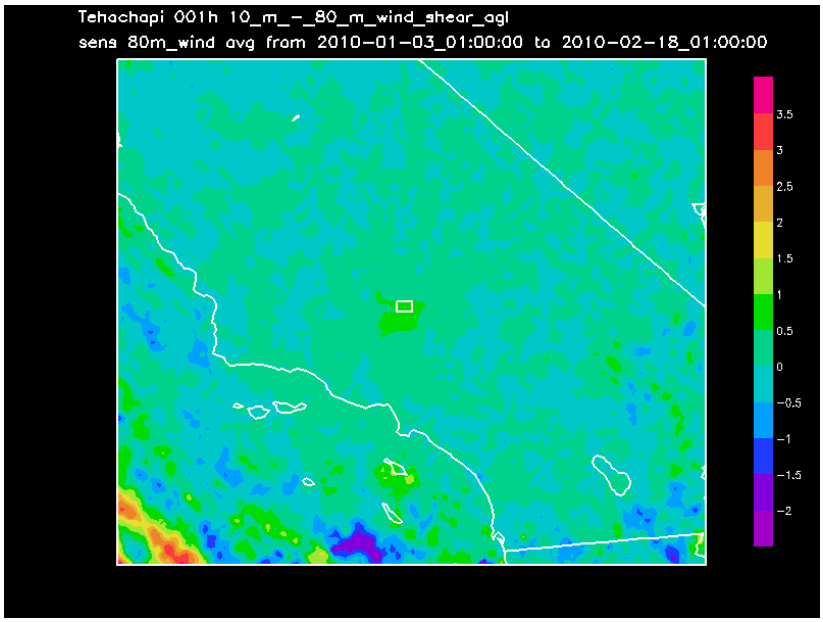

Figure C6. *Average sensitivity of 80-m wind speed (m/s) within the white target box to 10-m to 80-m AGL wind speed difference throughout the entire grid domain for a 1-hour ahead forecast during all time periods in the 46-day analysis period for Tehachapi.*

3-Hour Ahead

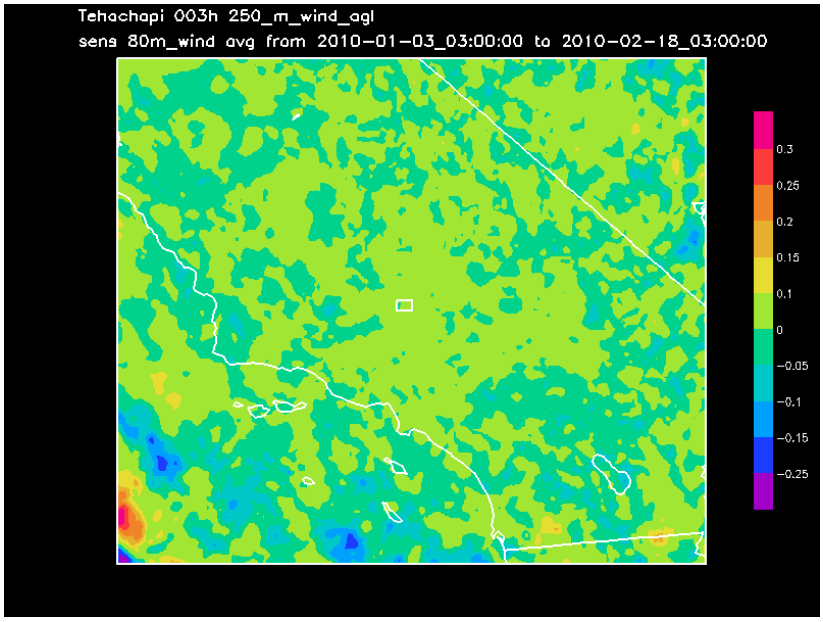

Figure C7. *Average sensitivity of 80-m wind speed (m/s) within the white target box to 250-m AGL wind speed (m/s) throughout the entire grid domain for a 1-hour ahead forecast during all time periods in the 46-day analysis period for Tehachapi.*

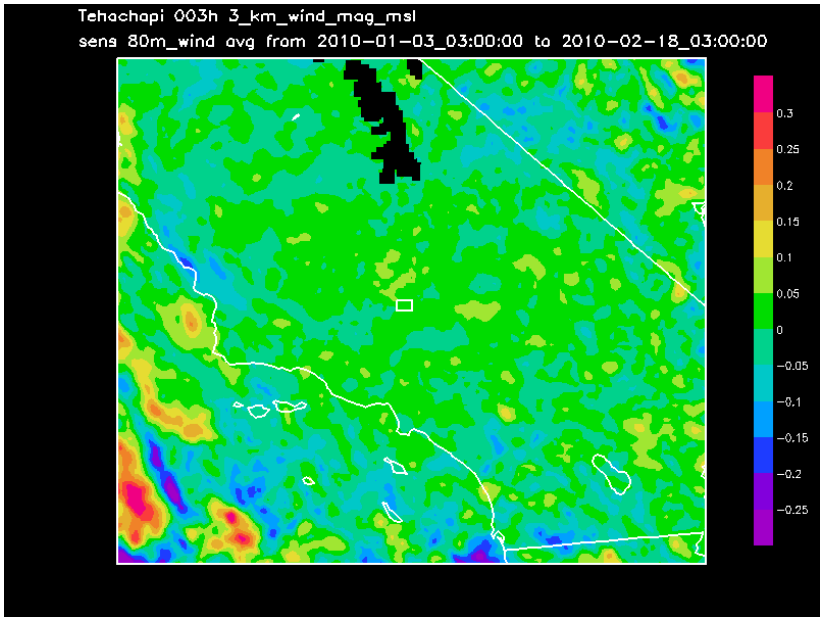

Figure C8. *Average sensitivity of 80-m wind speed (m/s) within the white target box to 3-km MSL wind speed (m/s) throughout the entire grid domain for a 3-hour ahead forecast during all time periods in the 46-day analysis period for Tehachapi.*

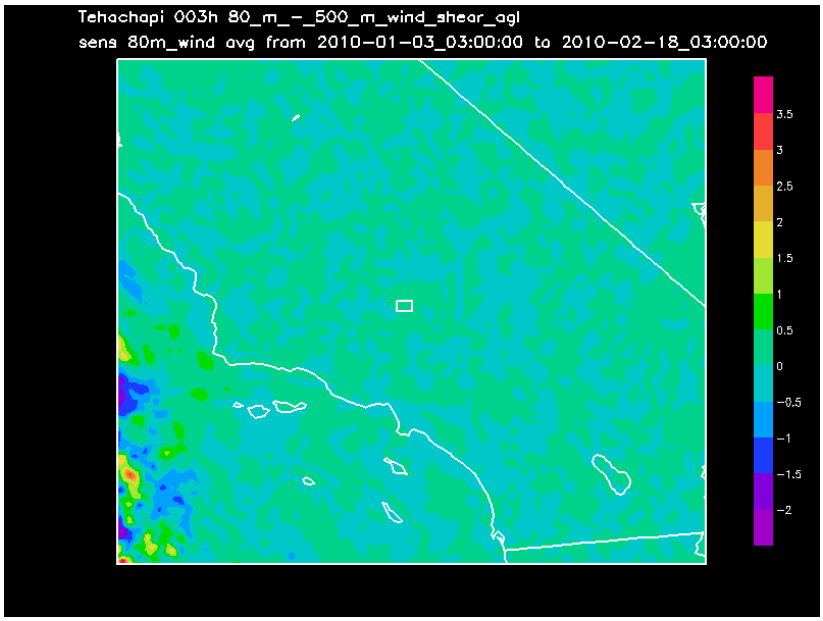

Figure C9. *Average sensitivity of 80-m wind speed (m/s) within the white target box to 80-m to 500-m AGL wind shear throughout the entire grid domain for a 3-hour ahead forecast during all time periods in the 46-day analysis period for Tehachapi.*

Appendix D: Additional Variable R^2 Sensitivity Results

1-Hour Ahead

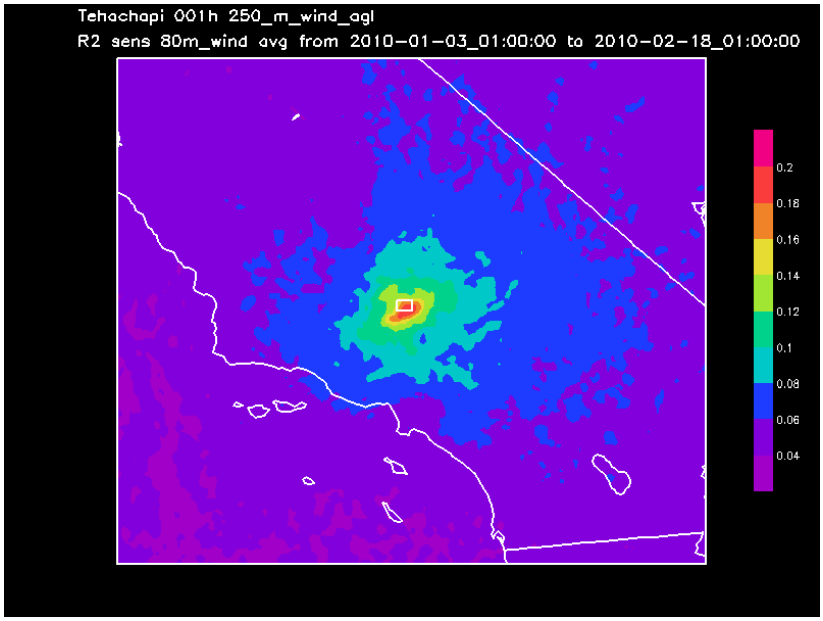

Figure D1. *Average R^2 sensitivity of 80-m wind speed (m/s) within the white target box to 250-m AGL wind speed (m/s) throughout the entire grid domain for a 1-hour ahead forecast during all time periods in the 46-day analysis period for Tehachapi.*

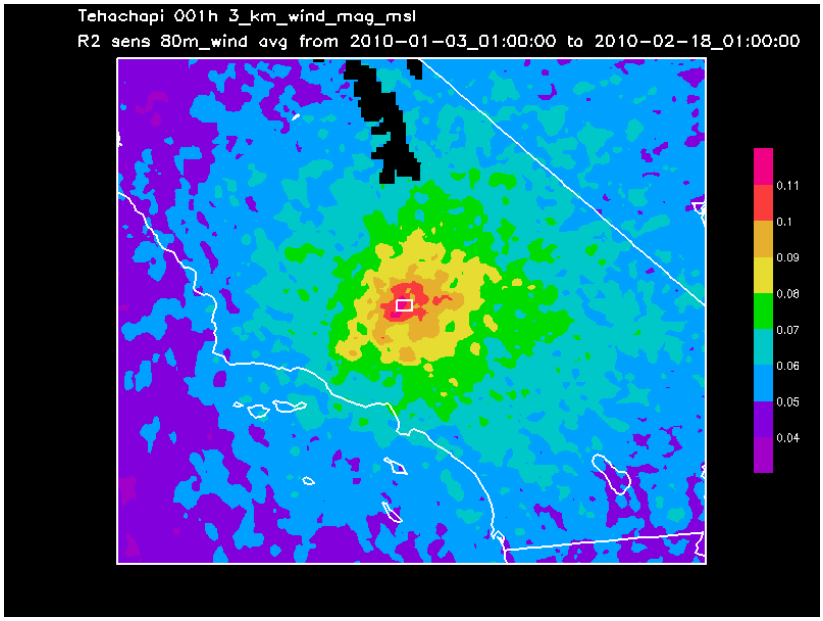

Figure D2. *Average R^2 sensitivity of 80-m wind speed (m/s) within the white target box to 3-km MSL wind speed (m/s) throughout the entire grid domain for a 1-hour ahead forecast during all time periods in the 46-day analysis period for Tehachapi.*

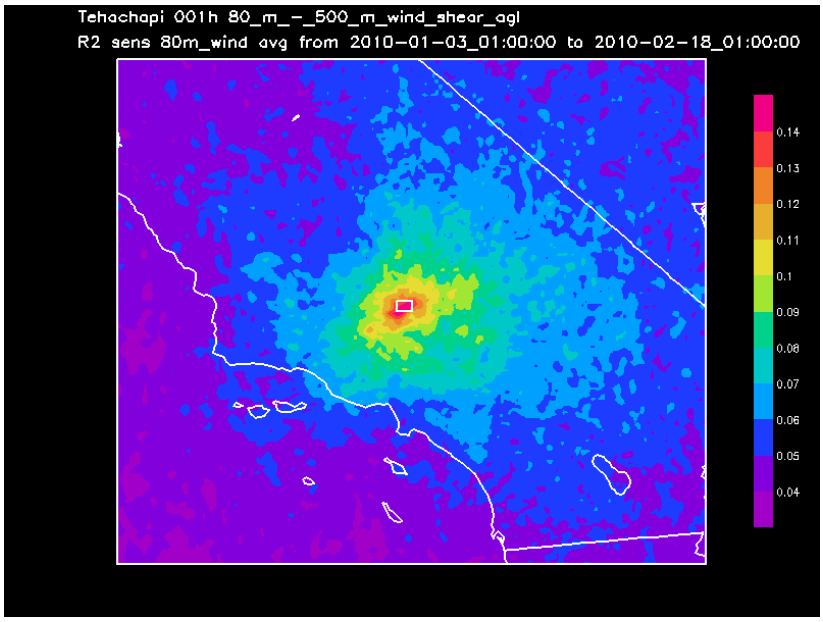

Figure D3. *Average R^2 sensitivity of 80-m wind speed (m/s) within the white target box to 80-m to 500-m AGL wind shear throughout the entire grid domain for a 1-hour ahead forecast during all time periods in the 46-day analysis period for Tehachapi.*

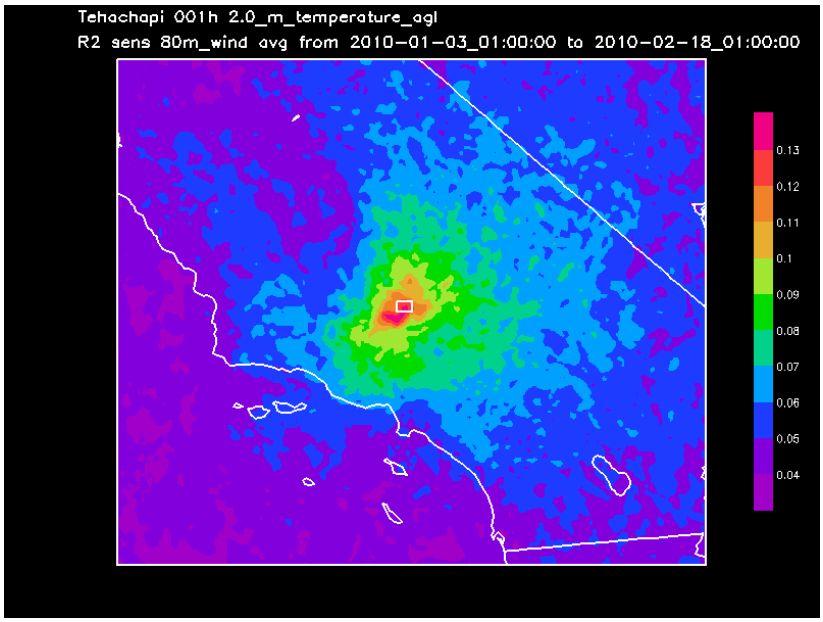

Figure D4. *Average R^2 sensitivity of 80-m wind speed (m/s) within the white target box to 80-m to 2-m AGL temperature throughout the entire grid domain for a 1-hour ahead forecast during all time periods in the 46-day analysis period for Tehachapi.*

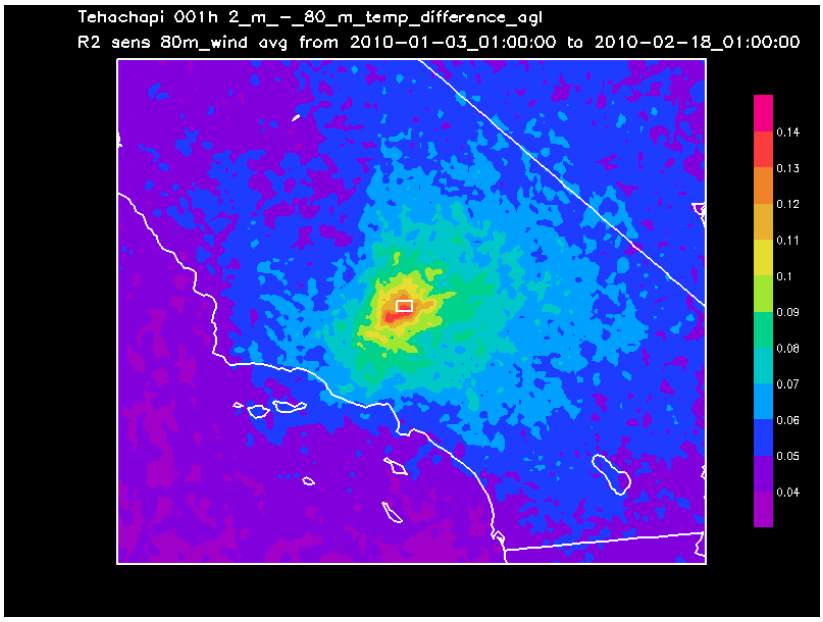

Figure D5. *Average R^2 sensitivity of 80-m wind speed (m/s) within the white target box to 2-m to 80-m AGL temperature difference throughout the entire grid domain for a 1-hour ahead forecast during all time periods in the 46-day analysis period for Tehachapi.*

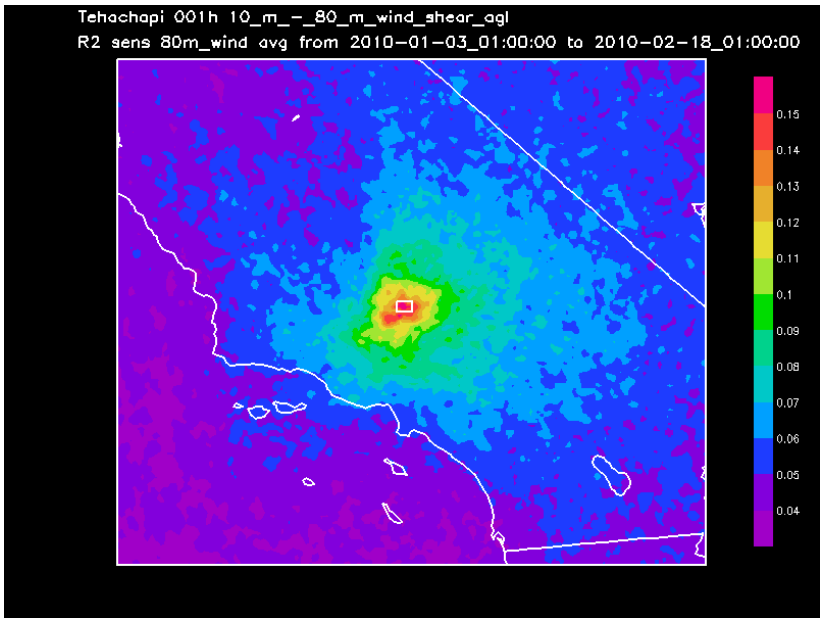

Figure D6. *Average R^2 sensitivity of 80-m wind speed (m/s) within the white target box to 10-m to 80-m AGL wind speed difference throughout the entire grid domain for a 1-hour ahead forecast during all time periods in the 46-day analysis period for Tehachapi.*

3-Hour Ahead

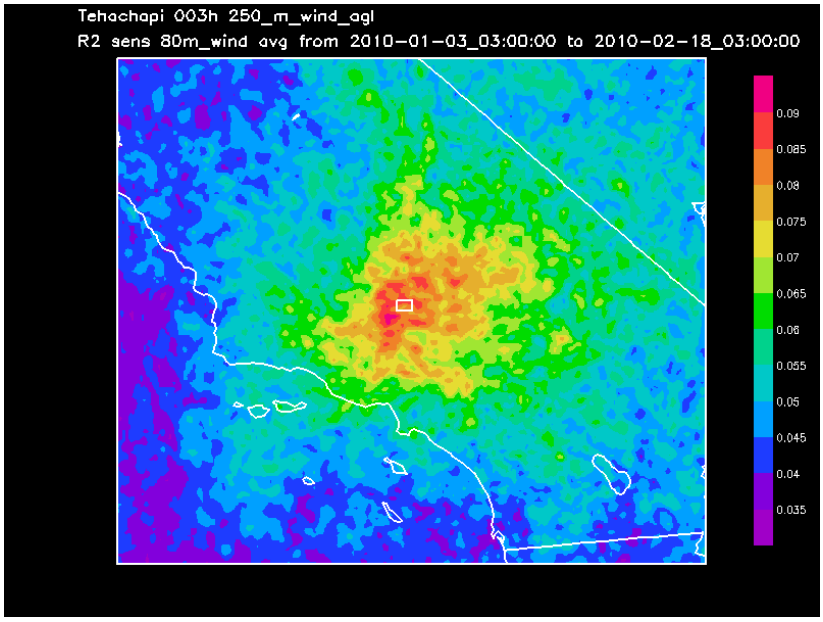

Figure D7. *Average R^2 sensitivity of 80-m wind speed (m/s) within the white target box to 250-m AGL wind speed (m/s) throughout the entire grid domain for a 3-hour ahead forecast during all time periods in the 46-day analysis period for Tehachapi.*

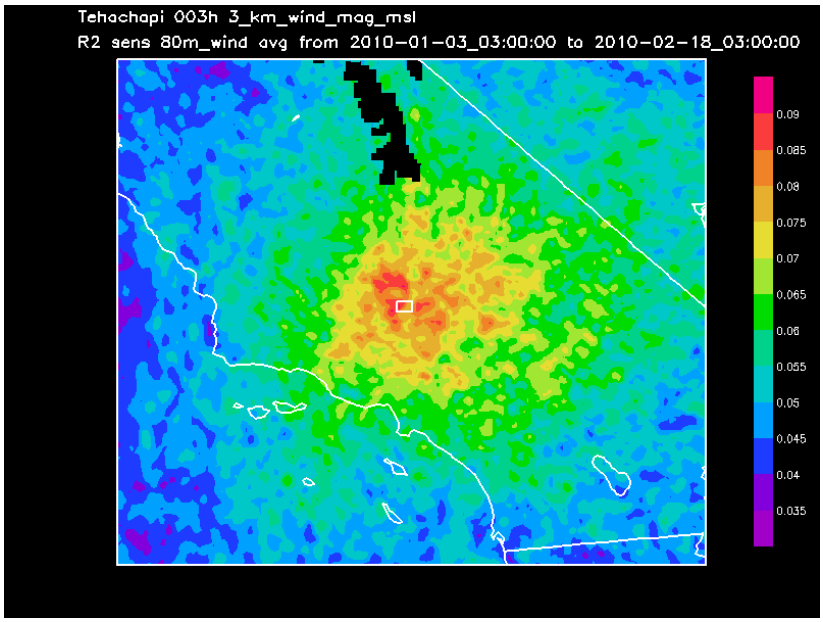

Figure D8. *Average R^2 sensitivity of 80-m wind speed (m/s) within the white target box to 3-km MSL wind speed (m/s) throughout the entire grid domain for a 3-hour ahead forecast during all time periods in the 46-day analysis period for Tehachapi.*

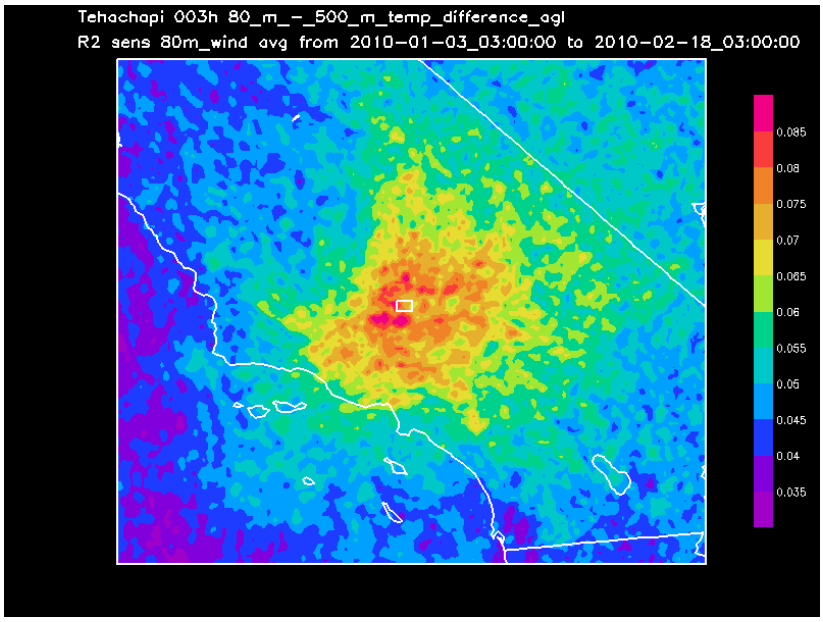

Figure D9. *Average R^2 sensitivity of 80-m wind speed (m/s) within the white target box to 80-m to 500-m AGL wind shear throughout the entire grid domain for a 3-hour ahead forecast during all time periods in the 46-day analysis period for Tehachapi.*

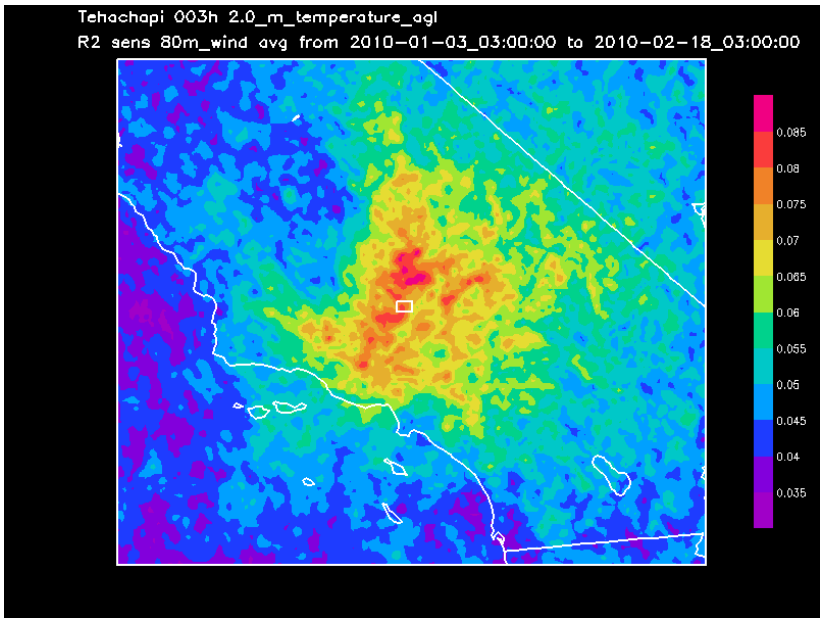

Figure D10. *Average R^2 sensitivity of 80-m wind speed (m/s) within the white target box to 2-m AGL temperature throughout the entire grid domain for a 3-hour ahead forecast during all time periods in the 46-day analysis period for Tehachapi.*

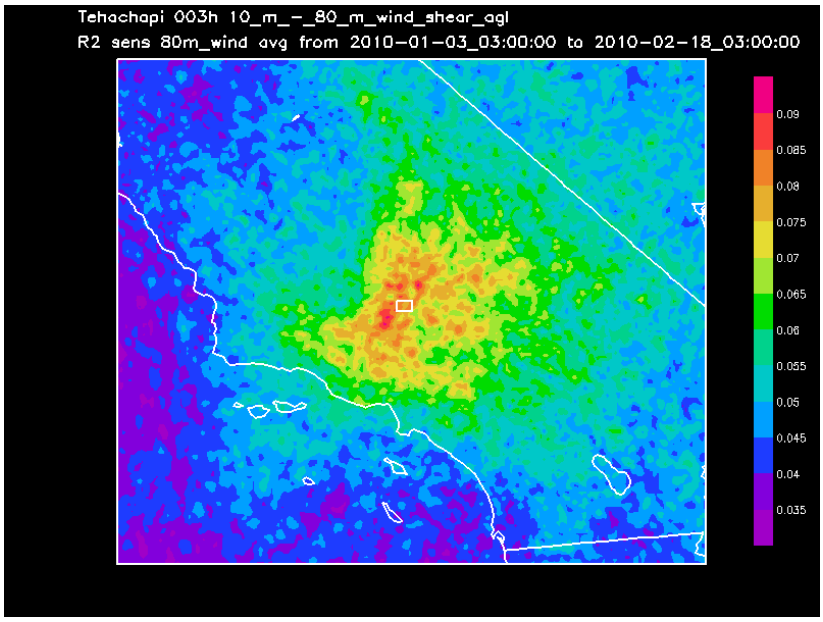

Figure D11. *Average R^2 sensitivity of 80-m wind speed (m/s) within the white target box to 10-m to 80-m AGL wind speed difference throughout the entire grid domain for a 3-hour ahead forecast during all time periods in the 46-day analysis period for Tehachapi.*

3 hour ahead – High Variance Cases

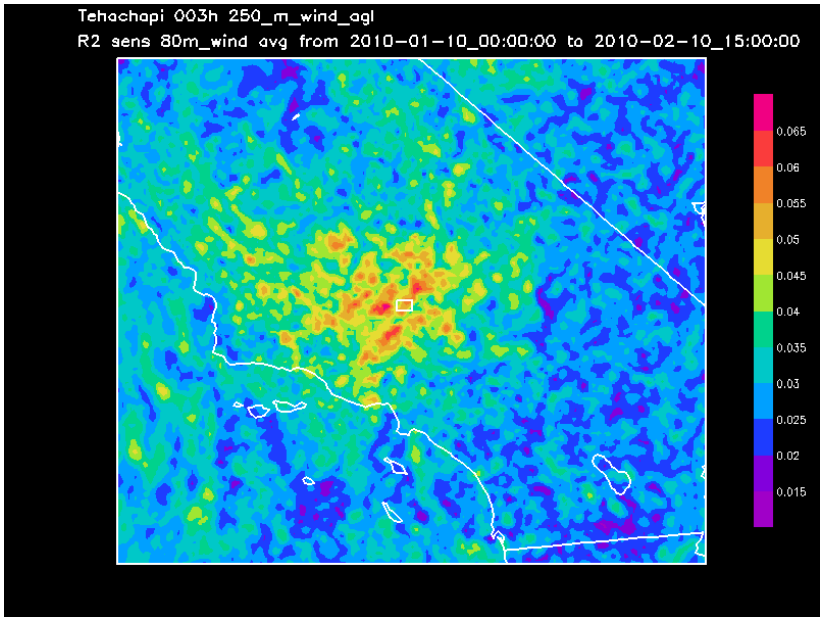

Figure D12. *Average R^2 sensitivity of 80-m wind speed (m/s) within the white target box to 250-m AGL wind speed (m/s) throughout the entire grid domain for a 3-hour ahead forecast during all time periods in the high variance analysis period for Tehachapi.*

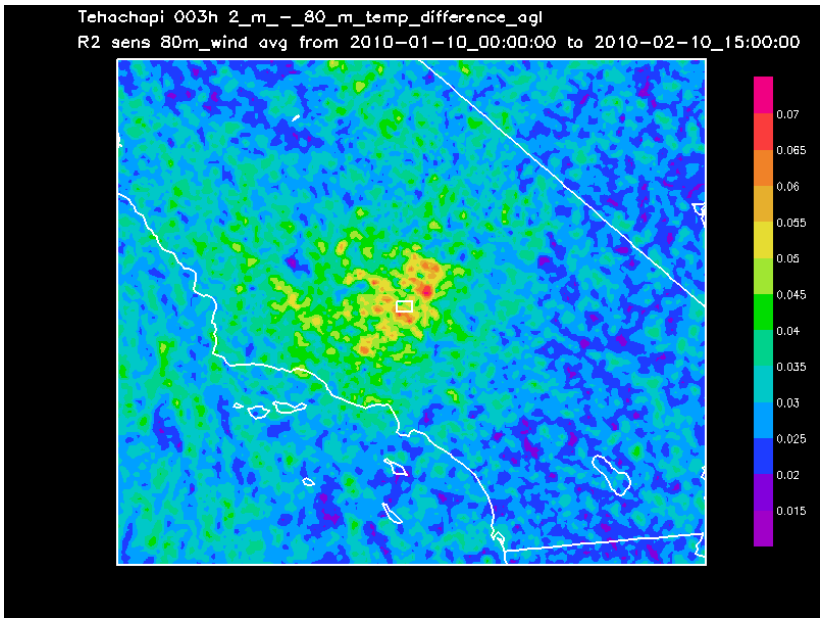

Figure D13. *Average R^2 sensitivity of 80-m wind speed (m/s) within the white target box to 2-m to 80-m AGL temperature difference throughout the entire grid domain for a 3-hour ahead forecast during all time periods in the high variance analysis period for Tehachapi.*

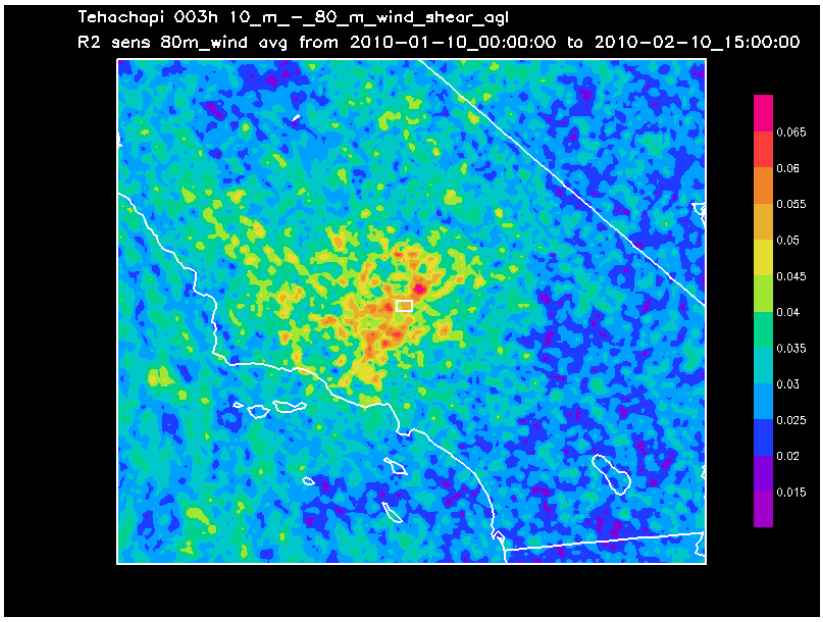

Figure D14. *Average R^2 sensitivity of 80-m wind speed (m/s) within the white target box to 10-m to 80-m AGL wind speed difference throughout the entire grid domain for a 3-hour ahead forecast during all time periods in high variance analysis period for Tehachapi.*

Appendix E: Additional Variable Significant Sensitivity Results

3-Hour Ahead

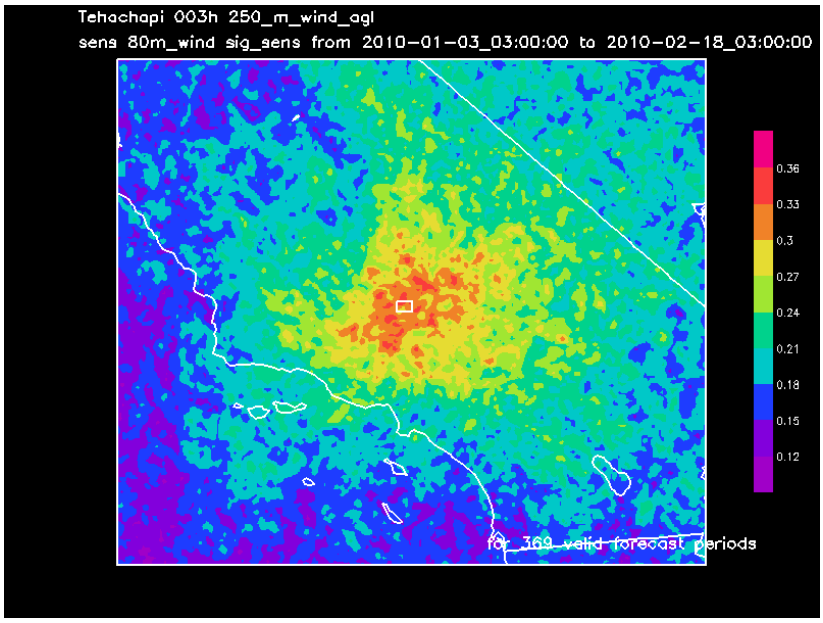

Figure E1. *Frequency (fraction of time periods) of statistically significant non-zero sensitivity at the 95% confidence level for average 80-m wind speed in the forecast metric area (white box) to 250-m wind speed 3 hours earlier for the 46-day sample.*

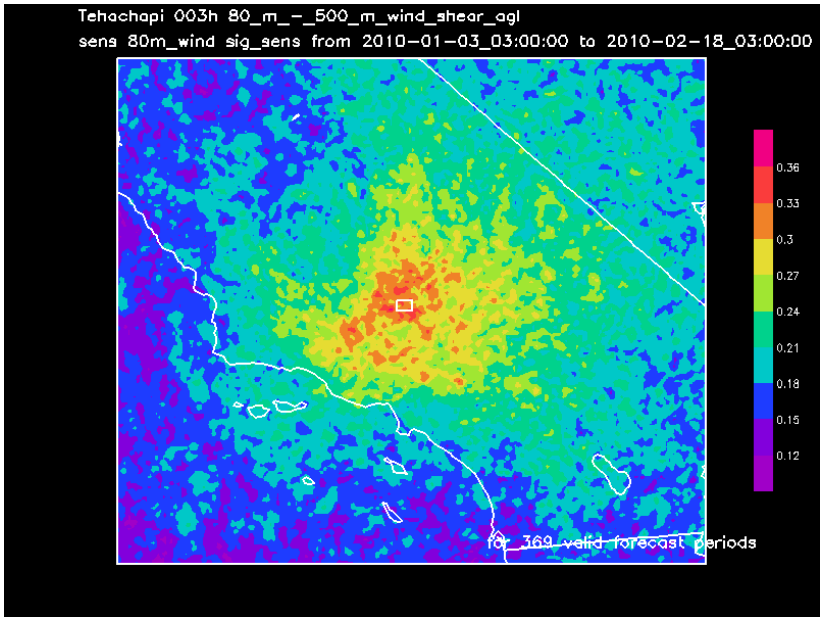

Figure E2. *Frequency (fraction of time periods) of statistically significant non-zero sensitivity at the 95% confidence level of the average 80-m wind speed in the forecast metric area (white box) to 80-m to 500-m AGL wind shear 3 hours earlier for the 46-day sample.*

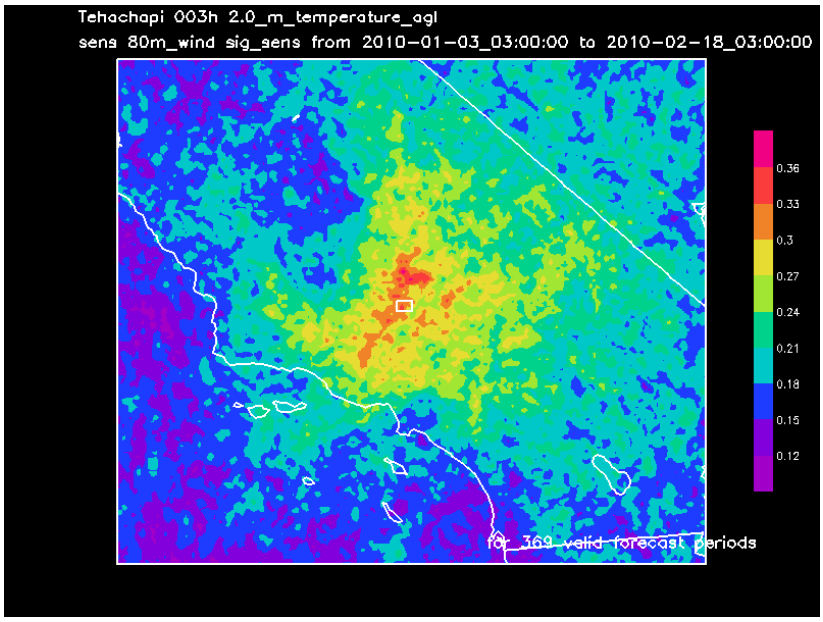

Figure E3. *Frequency (fraction of time periods) of statistically significant non-zero sensitivity at the 95% confidence level of the average 80-m wind speed in the forecast metric area (white box) to 2-m AGL temperature 3 hours earlier for the 46-day sample.*

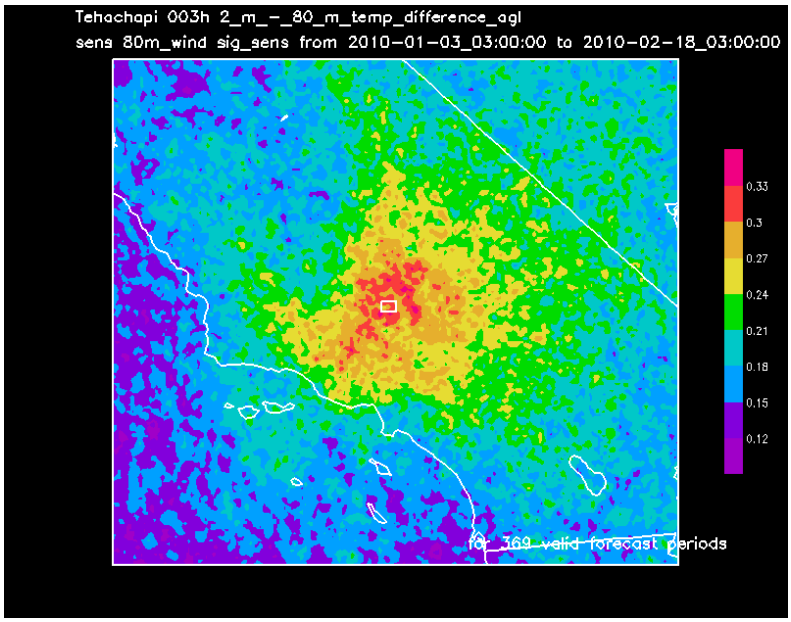

Figure E4. *Frequency (fraction of time periods) of statistically significant non-zero sensitivity at the 95% confidence level of the average 80-m wind speed in the forecast metric area (white box) to 2-m to 80-m AGL temperature difference 3 hours earlier for the 46-day sample.*

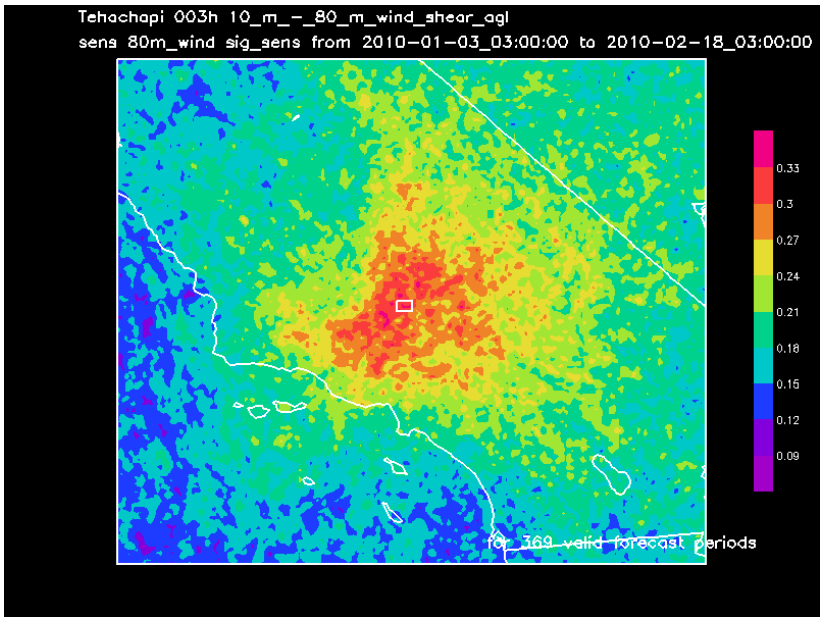

Figure E5. *Frequency (fraction of time periods) of statistically significant non-zero sensitivity at the 95% confidence level of the average 80-m wind speed in the forecast metric area (white box) to 10-m to 80-m AGL wind speed difference 3 hours earlier for the 46-day sample.*